Steel 8622 (8822 Low Side) Quenched Core (Vac.) Iteration #102 and 106

Monotonic Tensile and Fatigue Test Results Including Overload Tests

Prepared by:

S. McKelvey, J. Lindsey
and
A. Fatemi

Department of Mechanical, Industrial and Manufacturing Engineering
The University of Toledo
Toledo, Ohio 43606

Prepared for:
The AISI Bar Steel Applications Group

September 2009

American Iron and Steel Institute
2000 Town Center, Suite 320
Southfield, Michigan 48075
tel: 248-945-4777
fax: 248-352-1740
www.autosteel.org

TABLE OF CONTENTS

NOMENCLATURE

A_o, A_f	initial, final area	S	engineering stress
HB, HRB, HRC	Brinell, Rockwell B-Scale, Rockwell C-Scale Hardness number	YS, UYS, LYS, YS'	Monotonic yield, upper yield, lower yield, cyclic yield strength
b, c, n	fatigue strength, fatigue ductility, strain hardening exponent	YPE	yield point elongation
D_o, D_f	initial, final diameter	S_u	ultimate tensile strength
e	engineering strain	%EL	percent elongation
E, E'	monotonic, midlife cycle modulus of elasticity	%RA	percent reduction in area
K, K'	monotonic, cyclic strength coefficient	σ, σ_f, σ_f'	true stress, true fracture strength, fatigue strength coefficient
L_o, L_f	initial, final gage length	σ_a, σ_m, $\Delta\sigma$	stress amplitude, mean stress, stress range
$N_{50\%}$, $(N_f)_{10\%}$, $(N_f)_{50\%}$,	number of cycles to midlife, 10% load drop, 50% load drop,	ε_e, ε_p, ε	true elastic, plastic, total strain
$2N_f$	reversals to failure	ε_f, ε_f'	true fracture ductility, fatigue ductility coefficient
P_f, P_u	fracture, ultimate load	ε_a, ε_m, $\Delta\varepsilon$	strain amplitude, mean strain, strain range
R	strain ratio, neck radius	$\Delta\varepsilon_e$, $\Delta\varepsilon_p$	elastic, plastic strain range

NOMENCLATURE

$\sigma_{m,\ SC}$	small cycle mean stress,	$\sigma_{a,\ SC}$	small cycle stress amplitude,
$\sigma_{m,\ OL}$	overload cycle mean stress	$\sigma_{a,\ OL}$	overload cycle stress amplitude
$\varepsilon_{a,\ SC}$	small cycle strain amplitude	$(\Delta\varepsilon_p/2)_{SC}$	small cycle plastic strain amplitude,
$\varepsilon_{a,\ OL}$	overload cycle strain amplitude	$(\Delta\varepsilon_p/2)_{OL}$	overload plastic strain amplitude
$\varepsilon_{m,\ SC}$	small cycle mean strain	B, B_f	number of blocks in a periodic overload test, number of blocks to failure in a periodic overload test
N_{SC}, $N_{f,\ SC(eq)}$	number of small cycles in an overload block, calculated equivalent life of the small cycles in an overload test	$N_{f,\ OL}$	Constant amplitude life to failure at the strain amplitude used for the periodic overload cycle amplitude

UNIT CONVERSION TABLE

Measure	SI Unit	US Unit	from SI to US	from US to SI
Length	mm	in	1 mm = 0.03937 in	1 in = 25.4 mm
Area	mm^2	in^2	1 mm^2 = 0.00155 in^2	1 in^2 = 645.16 mm^2
Load	kN	klb	1kN = 0.2248 klb	1 klb = 4.448 kN
Stress	MPa	ksi	1 MPa = 0.14503 ksi	1 ksi = 6.895 MPa
Temperature	°C	°F	°C = (°F - 32)/1.8	°F = (°C * 1.8) + 32

In SI Unit:				
	1 kN = 10^3 N	1 Pa = 1 N/m^2	1 MPa = 10^6 Pa = 1 N/mm^2	1 Gpa = 10^9 Pa
In US Unit:				
	1 klb = 10^3 lb	1 psi = 1 lb/in^2	1 ksi = 10^3 psi	

SUMMARY

Monotonic tensile properties and fatigue behavior data were obtained for steel material of iterations 102 and 106. The material was provided by AISI. Two tensile tests were performed to acquire the desired monotonic properties. Both tests gave similar results. Eighteen strain-controlled fatigue tests were performed to obtain the fatigue life and cyclic deformation curves and properties. The experimental procedure followed and results obtained are presented and discussed in this report. Periodic overload fatigue behavior and data were also obtained from eight strain-controlled periodic overload fatigue tests. The experimental procedure followed and results obtained from periodic overload tests are also presented and discussed in this report.

I. EXPERIMENTAL PROGRAM

1.1 Material and Specimen Fabrication

1.1.1 Material

The steel material was provided by AISI. The test specimen was prepared from an 8822 steel grade with low side chemistry. The samples were quench and tempered by austenitizing at 1700F prior to gas quenching in nitrogen at 18 bar and then tempering at 350F to an aim hardness of 30-35 HRC (see Appendix B). Inclusion distribution and microstructure of the material are shown in Figures 1 and 2, respectively.

1.1.2 Specimen

In this study, identical round specimens were used for monotonic and fatigue tests. The specimen configuration and dimensions are shown in Figure 3. This configuration deviates slightly from the specimens recommended by ASTM Standard E606 [1]. The recommended specimens have uniform gage sections. The specimen geometry shown in Figure 3 differs by using a large secondary radius in the gage section to compensate for the slight stress concentration at the gage to grip section transition.

All specimens were machined in the Mechanical, Industrial, and Manufacturing Engineering Machine Shop at the University of Toledo. The specimens were initially turned on a lathe to an appropriate diameter for insertion into a CNC/milling machine. Using the CNC machine, final turning was performed to achieve the tolerable dimensions specified on the specimen drawings. Specimen straightness was checked on a flat stone.

The specimens were then polished prior to testing at the University of Toledo. A commercial round-specimen polishing machine was used to polish the specimen gage section. Three different grits of aluminum oxide lapping film 30 μm, 12 μm, and 3 μm were used. Polishing marks coincided with the longitudinal direction of the specimen. The polished surfaces were carefully examined under magnification to ensure complete removal of machine marks within the test section.

There was a large variation in measured hardness values of some specimens (about 10 points in HRC). As a result, data from five of the specimens tested were not used in data fits (see foot note in Table A.2).

1.2 Testing Equipment

1.2.1 Apparatus

An INSTRON 8801 closed-loop servo-controlled hydraulic axial load frame in conjunction with a Fast-Track digital servo-controller was used to conduct the tests. The load cell used had a capacity of 50 kN. Hydraulically operated grips using universal tapered collets were employed to secure the specimens' ends in series with the load cell.

An MST closed-loop servo-controlled hydraulic axial load frame in conjunction with a Fast-Track digital servo-controller was also used to conduct the tests. The load cell used had a capacity of 100 kN. Hydraulically operated grips using universal tapered wedges were employed to secure the specimens' ends in series with the load cell.

Total strain was controlled using an extensometer rated as ASTM class B1 [2]. The calibration of the extensometer was verified using displacement apparatus containing

a micrometer barrel in divisions of 0.0001 in. The extensometer had a gage length of 0.30 in. and was capable of measuring strains up to 15 %.

In order to protect the specimens' surface from the knife-edges of the extensometer, ASTM Standard E606 recommends the use of transparent tape or epoxy to 'cushion' the attachment. For this study, it was found that application of transparent tape strips was difficult due to the size of the test section. Therefore, epoxy was considered to be the best protection. The tests were performed using M-coat D.

1.2.2 Alignment

Significant effort was put forth to align the load train (load cell, grips, specimen, and actuator). Misalignment can result from both tilt and offset between the central lines of the load train components. In order to align the machine, a round strain-gage bar with two arrays of four strain gages per array that were arranged at the upper and lower ends of the uniform gage section was used. This was done in accordance with ASTM Standard E1012 [3].

1.3 Test Methods and Procedures

1.3.1 Monotonic tension tests

Monotonic tests in this study were performed using test methods specified by ASTM Standard E8 [4]. Two specimens were used to obtain the monotonic properties.

In order to protect the extensometer, strain control was used only up to 6% strain, until the point of ultimate tensile strength had been crossed. After this point, displacement control was used until fracture. INSTRON Bluehill software was used for

the monotonic tests. For the elastic and initial yield region (0% to 0.5% strain) as well as the period up to which the extensometer was removed, a strain rate of 0.0025 in/in/min was chosen. This strain rate was three-quarters of the maximum allowable rate specified by ASTM Standard E8 for the initial yield region. After the extensometer was removed, a displacement rate of 0.006 in/min was used.

After the tension tests were concluded, the broken specimens were carefully reassembled. The final gage lengths of the fractured specimens were measured with a Vernier caliper having divisions of 0.001 in. Using an optical comparator with 10X magnification and divisions of 0.001 in, the final diameter and neck radius were measured. It should be noted that prior to the test, the initial diameter was measured with this same instrument.

1.3.2 Constant amplitude fatigue tests

All constant amplitude fatigue tests in this study were performed according to ASTM Standard E606. It is recommended by this standard that at least 10 specimens be used to generate the fatigue properties. For this study, 18 specimens at 6 different strain amplitudes ranging from 0.275% to 2.00% were utilized. As mentioned previously, due to the large variation in measured hardness values of some specimens, data from five tests were not used to determine fatigue properties. INSTRON LCF software was used in all strain-controlled tests. During each strain-controlled test, the total strain was recorded using the extensometer output. Test data were automatically recorded throughout each test.

There were two control modes used for these tests. Strain control was used in all tests with plastic deformation. For one of the elastic tests, strain control was used initially

to determine the stabilized load, then load control was used for the remainder of the test and for the rest of the elastic tests, load control was used throughout. The reason for the change in control mode was due to the frequency limitation on the extensometer. For the strain-controlled tests, the applied frequencies ranged from 0.2 Hz to 5 Hz in order to keep a strain rate about 0.02 in/in/sec. For the load-controlled tests, load waveforms with frequencies of up to 24 Hz were used in order to shorten the overall test duration. All tests were conducted using a triangular waveform except the tests run at 24 Hz, when a sinusoidal waveform was used.

1.3.3 Periodic overload fatigue tests

The overload tests were conducted to investigate the effects of periodic overloads on the fatigue life of smaller subsequent cycles. For this study, 8 specimens were tested at 5 different strain amplitudes. The periodic overload tests were run in strain-control with INSTRON WAVERUNNER software. During each strain-controlled test, the total strain was recorded using the extensometer output. Test data were automatically recorded throughout each test

The input signal consisted of a periodic fully reversed overload of the type shown in Figure 13. The load history in these tests consisted of repeated load blocks made up of one fully-reversed overload cycle followed by a group of smaller constant amplitude cycles having the same maximum stress as the overload cycle. The overload cycles were applied at frequent intervals to maintain a low crack opening stress resulting in the subsequent cycles being fully open.

With this overload history, as the large cycles become more frequent, the fraction of the total damage done by them increases and that done by the small cycles decreases.

The fully reversed strain amplitude for the overload cycle corresponded to 10^4 cycles to failure. The number of small cycles per block, N_{sc}, were adjusted so that they cause 80 to 90% of the damage per block. Small cycle strain levels were selected at or below the run out level of the constant amplitude tests. Small cycles strain amplitudes were used from 0.275% to 0.100% and the number of small cycles per overload cycle ranged between 30 and 1000.

II. Experimental results and analysis

2.1 Microstructural Data

A fatigue specimen was sectioned transversely thru the gage section and longitudinally thru the grip section. The samples were prepared with standard lab procedures for sectioning, mounting, grinding, polishing and etched with 3% Nital. Photomicrographs were taken using a Nikon Epiphot 200 microscope and Image-Pro Plus was used to estimate case depth. The microstructure consisted of tempered martensite from surface to core. There appeared to be some centerline segregation and banding in the sample (see Appendix B). The chemistry of the material is presented in Table 1. Figure 1 shows a photo of the inclusion distribution in the steel and Figure 2 shows a high magnification view of the microstructure from the gage area. The complete material report for this steel was provided by the Chrysler Materials Engineering Lab and is attached as Appendix B of this report.

2.2 Monotonic Deformation Behavior

The properties determined from monotonic tests were the following: modulus of elasticity (E), yield strength (YS), ultimate tensile strength (S_u), percent elongation

(%EL), percent reduction in area (%RA), true fracture strength (σ_f), true fracture ductility (ε_f), strength coefficient (K), and strain hardening exponent (n).

True stress (σ), true strain (ε), and true plastic strain (ε_p) were calculated from engineering stress (S) and engineering strain (e), according to the following relationships which are based on constant volume assumption:

$$\sigma = S(1+e) \tag{1a}$$

$$\varepsilon = \ln(1+e) \tag{1b}$$

$$\varepsilon_p = \varepsilon - \varepsilon_e = \varepsilon - \frac{\sigma}{E} \tag{1c}$$

The true stress (σ) - true strain (ε) plot is often represented by the Ramberg-Osgood equation:

$$\varepsilon = \varepsilon_e + \varepsilon_p = \frac{\sigma}{E} + \left(\frac{\sigma}{K}\right)^{\frac{1}{n}} \tag{2}$$

The strength coefficient, K, and strain hardening exponent, n, are the intercept and slope of the best line fit to true stress (σ) versus true plastic strain (ε_p) data in log-log scale:

$$\sigma = K\left(\varepsilon_p\right)^n \tag{3}$$

In accordance with ASTM Standard E739 [5], when performing the least squares fit, the true plastic strain (ε_p) was the independent variable and the true stress (σ) was the dependent variable. These plots for the two tests conducted are shown in Figure 4. To generate the K and n values, the range of data used in this figure was chosen according to the definition of discontinuous yielding specified in ASTM Standard E646 [6]. Therefore,

the valid data range occurred between the end of yield point extension and the strain at maximum load.

The true fracture strength was corrected for necking according to the Bridgman correction factor [7]:

$$\sigma_f = \frac{\frac{P_f}{A_f}}{\left[1+\frac{4R}{D_f}\right]\ln\left[1+\frac{D_f}{4R}\right]} \tag{4}$$

where P_f is load at fracture, R is the neck radius, and D_f is the diameter at fracture.

The true fracture ductility, ε_f, was calculated from the relationship based on constant volume:

$$\varepsilon_f = \ln\left(\frac{A_o}{A_f}\right) = \ln\left(\frac{1}{1-RA}\right) \tag{5}$$

where A_f is the cross-sectional area at fracture, A_o is the original cross-sectional area, and RA is the reduction in area.

A summary of the monotonic properties for this material is provided in Table A.1. The monotonic stress-strain curves are shown in Figure 5. As can be seen from this figure, the two curves are very close to each other. Refer to Table A.1 for a summary of the monotonic test results.

2.3 Cyclic Deformation Behavior

2.3.1 Transient cyclic response

Transient cyclic response describes the process of cyclic-induced change in deformation resistance of a material. Data obtained from constant amplitude strain-controlled fatigue tests were used to determine this response. Plots of stress amplitude variation versus applied number of cycles can indicate the degree of transient cyclic softening/hardening. Also, these plots show when cyclic stabilization occurs. A composite plot of the transient cyclic response for the steel studied is shown in Figure A.1. The transient response was normalized on the rectangular plot in Figure A.1a, while a semi-log plot is shown in Figure A.1b. Even though multiple tests were conducted at each strain amplitude, data from one test at each strain amplitude tested are shown in these plots.

2.3.2 Steady-state cyclic deformation

Another cyclic behavior of interest was the steady state or stable response. Data obtained from constant amplitude strain-controlled fatigue tests were also used to determine this response. The properties determined from the steady-state hysteresis loops were the following: cyclic modulus of elasticity (E'), cyclic strength coefficient (K'), cyclic strain hardening exponent (n'), and cyclic yield strength (YS'). Half-life (midlife) hysteresis loops and data were used to obtain the stable cyclic properties.

Similar to monotonic behavior, the cyclic true stress-strain behavior can be characterized by the Ramberg-Osgood type equation:

$$\frac{\Delta\varepsilon}{2} = \frac{\Delta\varepsilon_e}{2} + \frac{\Delta\varepsilon_p}{2} = \frac{\Delta\sigma}{2E} + \left(\frac{\Delta\sigma}{2K'}\right)^{\frac{1}{n'}} \quad (6)$$

It should be noted that in Equation 6 and the other equations that follow, E is the average modulus of elasticity that was calculated from the monotonic tests.

The cyclic strength coefficient, K', and cyclic strain hardening exponent, n', are the intercept and slope of the best line fit to true stress amplitude ($\Delta\sigma/2$) versus true plastic strain amplitude ($\Delta\varepsilon_p/2$) data in log-log scale:

$$\frac{\Delta\sigma}{2} = K'\left(\frac{\Delta\varepsilon_p}{2}\right)^{n'} \quad (7)$$

In accordance with ASTM Standard E739 [5], when performing the least squares fit, the true plastic strain amplitude ($\Delta\varepsilon_p/2$) was the independent variable and the stress amplitude ($\Delta\sigma/2$) was the dependent variable. The true plastic strain amplitude was calculated by the following equation:

$$\frac{\Delta\varepsilon_p}{2} = \frac{\Delta\varepsilon}{2} - \frac{\Delta\sigma}{2E} \quad (8)$$

This plot is shown in Figure 6. To generate the K' and n' values, the range of data used in this figure was chosen for $\left[\frac{\Delta\varepsilon_p}{2}\right]_{calculated} \geq 0.00032$ in/in.

The cyclic stress-strain curve reflects the resistance of a material to cyclic deformation and can be vastly different from the monotonic stress-strain curve. The cyclic stress-strain curve is shown in Figure 7. In Figure 8, superimposed plots of monotonic and cyclic curves are shown. As can be seen in this figure, the material cyclically softened. Figure A.2 shows a composite plot of the steady-state (midlife)

hysteresis loops. Even though multiple tests were conducted at each strain amplitude, the stable loops from only one test at each strain amplitude are shown in this plot.

2.4 Constant Amplitude Fatigue Behavior

Constant amplitude strain-controlled fatigue tests were performed to determine the strain-life curve. The following equation relates the true strain amplitude to the fatigue life:

$$\frac{\Delta\varepsilon}{2}=\frac{\Delta\varepsilon_e}{2}+\frac{\Delta\varepsilon_p}{2}=\frac{\sigma_f'}{E}(2N_f)^b+\varepsilon_f'(2N_f)^c \qquad (9)$$

where σ_f' is the fatigue strength coefficient, b is the fatigue strength exponent, ε_f' is the fatigue ductility coefficient, c is the fatigue ductility exponent, E is the monotonic modulus of elasticity, and $2N_f$ is the number of reversals to failure.

The fatigue strength coefficient, σ_f', and fatigue strength exponent, b, are the intercept and slope of the best line fit to true stress amplitude ($\Delta\sigma/2$) versus reversals to failure ($2N_f$) data in log-log scale:

$$\frac{\Delta\sigma}{2}=\sigma_f'(2N_f)^b \qquad (10)$$

In accordance with ASTM Standard E739, when performing the least squares fit, the stress amplitude ($\Delta\sigma/2$) was the independent variable and the reversals to failure ($2N_f$) was the dependent variable. This plot is shown in Figure 9. To generate the σ_f' and b values, all data, with the exception of the five tests not used due to hardness variation and the run-out tests, in the stress-life figure were used.

The fatigue ductility coefficient, ε_f', and fatigue ductility exponent, c, are the intercept and slope of the best line fit to calculated true plastic strain amplitude ($\Delta\varepsilon_p/2$) versus reversals to failure ($2N_f$) data in log-log scale:

$$\left(\frac{\Delta\varepsilon_p}{2}\right)_{calculated} = \varepsilon_f'(2N_f)^c \qquad (11)$$

In accordance with ASTM Standard E739, when performing the least squares fit, the calculated true plastic strain amplitude ($\Delta\varepsilon_p/2$) was the independent variable and the reversals to failure ($2N_f$) was the dependent variable. The calculated true plastic strain amplitude was determined from Equation 8. This plot is shown in Figure 10. To generate the ε_f' and c values, the range of data used in this figure was chosen for $\left[\frac{\Delta\varepsilon_p}{2}\right]_{calculated} \geq 0.00032$ in/in.

The true strain amplitude versus reversals to failure plot is shown in Figure 11. This plot displays the strain-life curve (Eqn. 9), the elastic strain portion (Eqn. 10), the plastic strain portion (Eqn. 11), and superimposed fatigue data. A summary of the cyclic properties for this steel is provided in Table 2. Table A.2 provides the summary of the fatigue test results.

A parameter often used to characterize fatigue behavior at stress concentrations, such as at the root of a notch, is Neuber parameter [7]. Neuber's stress range is given by:

$$\sqrt{(\Delta\varepsilon)(\Delta\sigma)E} = 2\sqrt{(\sigma_f')^2(2N_f)^{2b} + \sigma_f'\varepsilon_f'E(2N_f)^{b+c}} \qquad (12)$$

A plot of Neuber stress range versus reversals to failure is shown in Figure 12. This figure displays the Neuber curve based on Eqn. 12 and superimposed fatigue data for this material

2.5 Periodic Overload Fatigue Behavior

Periodic Overload strain-controlled fatigue tests were performed to determine the effective strain-life curve. The effective strain-life curve is plotted using the strain amplitude of the small cycles in the overload block and the calculated equivalent life. The equivalent fatigue lives for the smaller cycles were obtained using the linear damage rule:

$$\frac{N_{OL}}{N_{f,OL}} + \frac{N_{SC}}{N_{f,SC(eq)}} = 1 \qquad (13)$$

where N_{OL} is the number of overload cycles in a periodic overload test, $N_{f,OL}$ is the number of cycles to failure if only overloads were applied in a test, N_{SC} is the number of smaller cycles in a periodic overload test, and $N_{f,SC(eq)}$ is the computed equivalent fatigue life for the smaller cycles.

The linear damage rule was also used to calculate the cumulative damage of the overload cycles, D_{OL}, as

$$\frac{N_{OL}}{N_{f,OL}} = D_{OL} \qquad (14)$$

Figure 14 shows the effective strain-life data superimposed on the constant amplitude strain life plot. Table A.3 presents a summary of the periodic overload test results.

A plot of the SWT parameter for both the constant amplitude and overload data provides another method of comparison between the two sets of data, where the mean stress present in the small cycles is taken into account. The SWT parameter is given by

$$\sigma_{\max}\varepsilon_a = \frac{1}{E}[(\sigma_f')^2(2N_f)^{2b} + \sigma_f'\varepsilon_f' E(2N_f)^{b+c}] \qquad (15)$$

where $\sigma_{max} = \sigma_m + \sigma_a$. The SWT plot is shown in Figure 15. As in the constant amplitude strain-life curve, the overload data and effective strain-life curve diverged from the constant amplitude curve.

Plots of the overload cycle and small cycle stress amplitude variation versus applied number of blocks can indicate the degree of transient cyclic softening/hardening. Also, these plots show when cyclic stabilization occurs over the life of the specimen. A composite plot of the small cycle transient cyclic response for the steel studied is shown in Figures A.3. A composite plot of the overload cycle transient cyclic response is shown in Figure A.4. The amplitude of the transient response is shown in the Figures A.3a and A.4a while the mean of the transient response is shown in Figures A.3b and A.4b. Even though multiple tests were conducted at each strain amplitude, data from one test at each strain amplitude tested are shown in these plots. While small cycle stress amplitude was constant during each test (Figure A3.a), there was significant increase in small cycle mean stress (Figure A3.b). The overload stress amplitude reduced significantly during life (i.e. cyclic softening), while the overload mean stress continued to increase (and decrease in one case) till failure (see Figure A.4b).

Stress response of small cycles was also evaluated within a single block. This can be seen in Figure A.5b, which is a plot of the mean stress at each strain level within a single block at midlife and in Figure A.5a, which shows the stress amplitude at each strain level within a single block at midlife. Once again, although multiple tests were conducted at each strain amplitude, data from one test at each strain amplitude tested are shown in these plots. These plots show steady state stress response within a load block.

The midlife hysteresis loops for each small cycle strain level are shown in Figures A.6a through A.6e. The small cycle loop was taken from the mid-cycle of the midlife block.

Additional testing was performed in order to verify the effectiveness of a strictly load-controlled test procedure. The majority of the test procedure is similar to the periodic overload procedure used in the strain controlled periodic overload tests. The load history consisted of a single overload cycle followed by a certain number of smaller cycles with the same maximum stress. For the load-controlled tests, calculations were performed based on equation 6 in order to arrive at the steady state stress amplitudes for the desired strain amplitudes. Due to the transient response of the material, the calculated loads would result in a lower than expected strain amplitude throughout the test. In order to reduce cyclic transient behavior, 1000 pre-cycles were applied at the periodic overload stress level. After completion of these initial cycles the second portion of the test was started using the previously mentioned periodic overload history. Three load-controlled tests were performed at load levels with expected strain levels of 0.275%, 0.150% and 0.100%. The results of these tests are included in Table A.3. In order to compare the life for the material obtained from this test procedure, the load-controlled periodic overload data were added to the strain-life and SWT curves. The result for the strain-life plot is shown in Figure 16 and for the SWT plot is in Figure 17.

Although load control was used throughout this test procedure, an extensometer was used to collect the strain levels occurring throughout the test. After the completion of the tests, the actual strain levels were compared with the expected strain levels. The results of this comparison are shown in Figure A.7. This plot shows that only a small

difference, if any, can be seen for the smaller cycles, but there was a larger variation in the strain levels for the overload cycles. This is to be expected though, due to the number of overload cycles before failure being less than the number of cycles it took to reach the steady state of stress in the constant amplitude testing.

Using this load-controlled periodic overload procedure did provide similar life values as were recorded for the strain-controlled tests. The only variation seen from the strain-controlled testing performed here is that the values for the life of the specimen were slightly longer in the load-controlled testing.

Table 1: Chemical Composition of 8622 (8822 Low Side) Steel (Courtesy of Chrysler)

Element	Wt. %
Carbon, C	0.210%
Manganese, Mn	0.810%
Phosphorus, P	0.020%
Sulfur, S	0.026%
Silicon, Si	0.260%
Chromium, Cr	0.500%
Aluminum, Al	0.031%
Nickel, Ni	0.460%
Molybdenum, Mo	0.250%
Copper, Cu	0.180%
Tin, Sn	0.010%
Vanadium, V	0.005%
Niobium, Nb	0.002%
Dl	2.260%

Table 2: Summary of the Mechanical Properties

Microstructural Data	Average
ASTM grain size number (MAG=500X):	
First longitudinal direction (L-T)	Fine grain 5 - 8
Inclusion rating number (MAG=100x): (Provided by Macsteel Company)	
Type A (sulfide type), thin series	-
Type B (alumina type), thin & heavy series	-
Type C (silicate type, thin & heavy series	-
Type D (globular type), thin & heavy series	-
Hardness:	
Brinell (HB)(converted)	
the first longitudinal direction	-
Transverse direction	301
Rockwell B-scale (HRB)	
The first longitudinal direction	-
Transverse direction	-
Rockwell C-scale (HRC)(measured)	
The first longitudinal direction	-
Transverse direction	32
Microstructure type:	
The first longitudinal direction	tempered martensite
Transverse direction	

Monotonic Properties	Average		Range	
Modulus of elasticity, E, GPa (ksi):	210.0	(30,457)	210.5 - 209.5	(30,524) - (30,391)
Yield strength (0.2% offset), YS , MPa (ksi):	990.0	(143.6)	990.0 - 990.0	(143.6 - 143.6)
Upper yield strength UYS, MPa (ksi):	-	-	- - -	- - -
Lower yield strength LYS, MPa (ksi):	-	-	- - -	- - -
Yield point elongation, YPE (%):	-	-	- - -	- - -
Ultimate strength, S_u , MPa (ksi):	1334.7	(193.6)	1343.4 - 1326.1	(194.8 - 192.3)
Percent elongation, %EL (%):	23.8%		24.3% - 23.4%	
Percent reduction in area, %RA (%):	46.9%		47.5% - 46.3%	
Strength coefficient, K , MPa (ksi):	2,305.7	(334.4)	2,186.9 - 2,424.5	(317.2 - 351.6)
Strain hardening exponent, n:	0.1443		0.1318 - 0.1567	
True fracture strength, σ_f , MPa (ksi):	1542.3	(223.7)	1562.6 - 1521.9	(226.6 - 220.7)
True fracture ductility, ε_f (%):	63.3%		64.4% - 62.2%	

Cyclic Properties	Average		Range	
Cyclic modulus of elasticity, E' , GPa (ksi):	201.5	(29,221)	205.0 - 198.9	(29,732) - (28,840)
Fatigue strength coefficient, σ_f' , MPa (ksi):	1,993.6	(289.1)		
Fatigue strength exponent, b:	-0.0888			
Fatigue ductility coefficient, ε_f' :	0.763			
Fatigue ductility exponent, c:	-0.6874			
Cyclic strength coefficient, K' , MPa (ksi):	1,899.8	(275.5)		
Cyclic strain hardening exponent, n':	0.1140			
Cyclic yield strength, YS', MPa (ksi)	935.7	(135.7)		
Fatigue Limit (defined at 10^6 cycles), Mpa (ksi)	549.3	(79.7)		

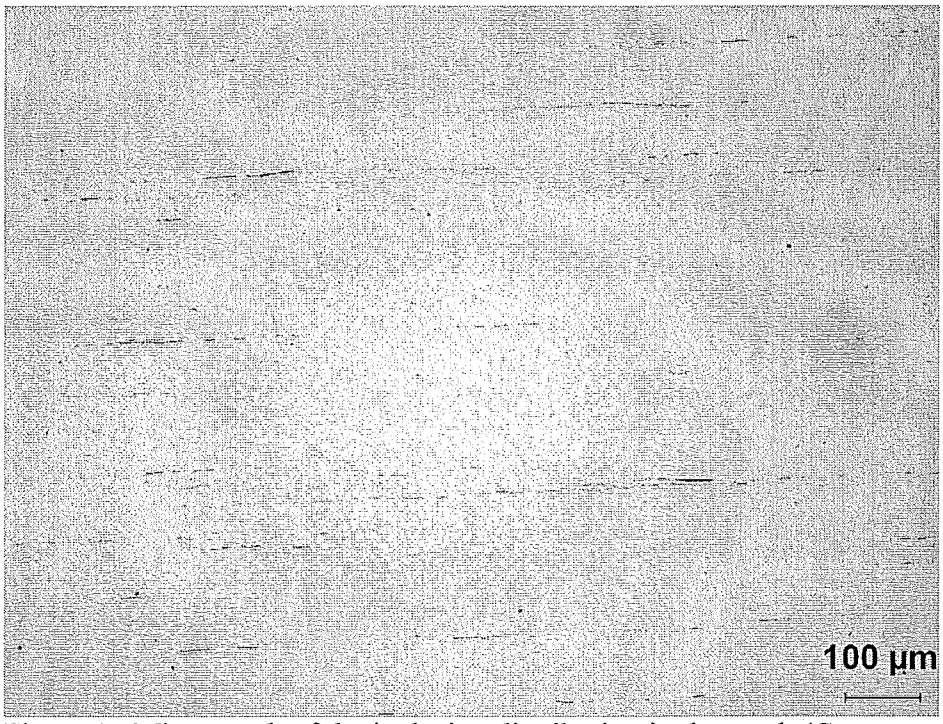

Figure 1: Micrograph of the inclusion distribution in the steel. (Courtesy of Chyrsler)

Figure 2: High magnification photo showing the microstructure of the transverse section from the gage area. (Courtesy of Chyrsler)

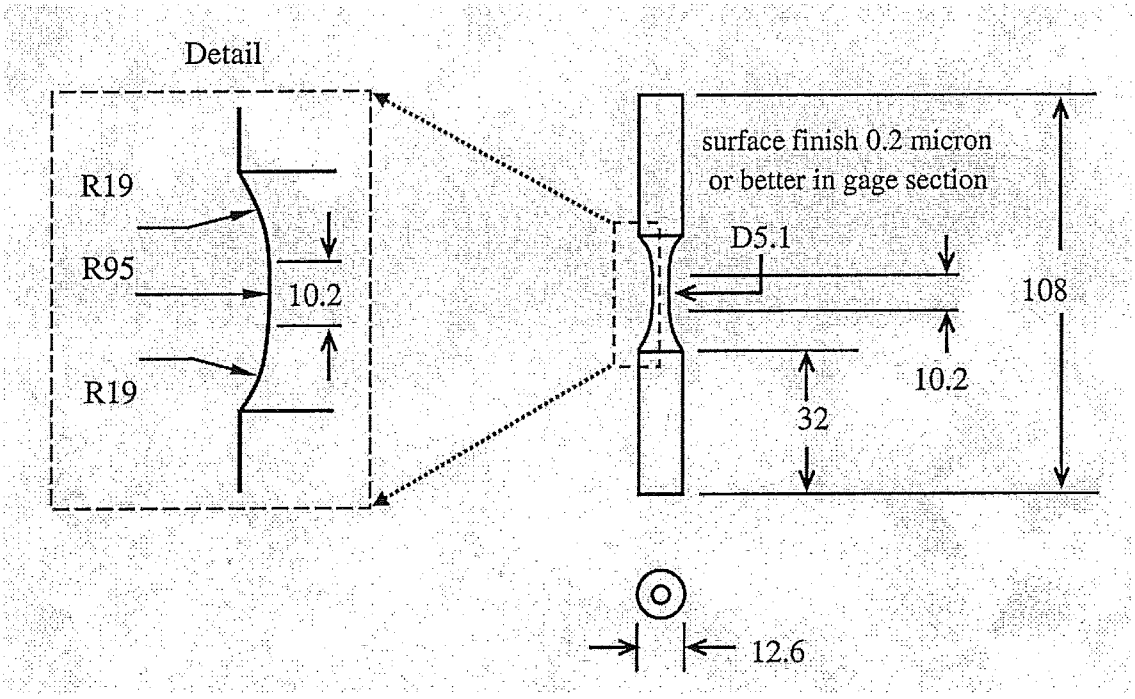

Figure 3: Specimen configuration and dimensions

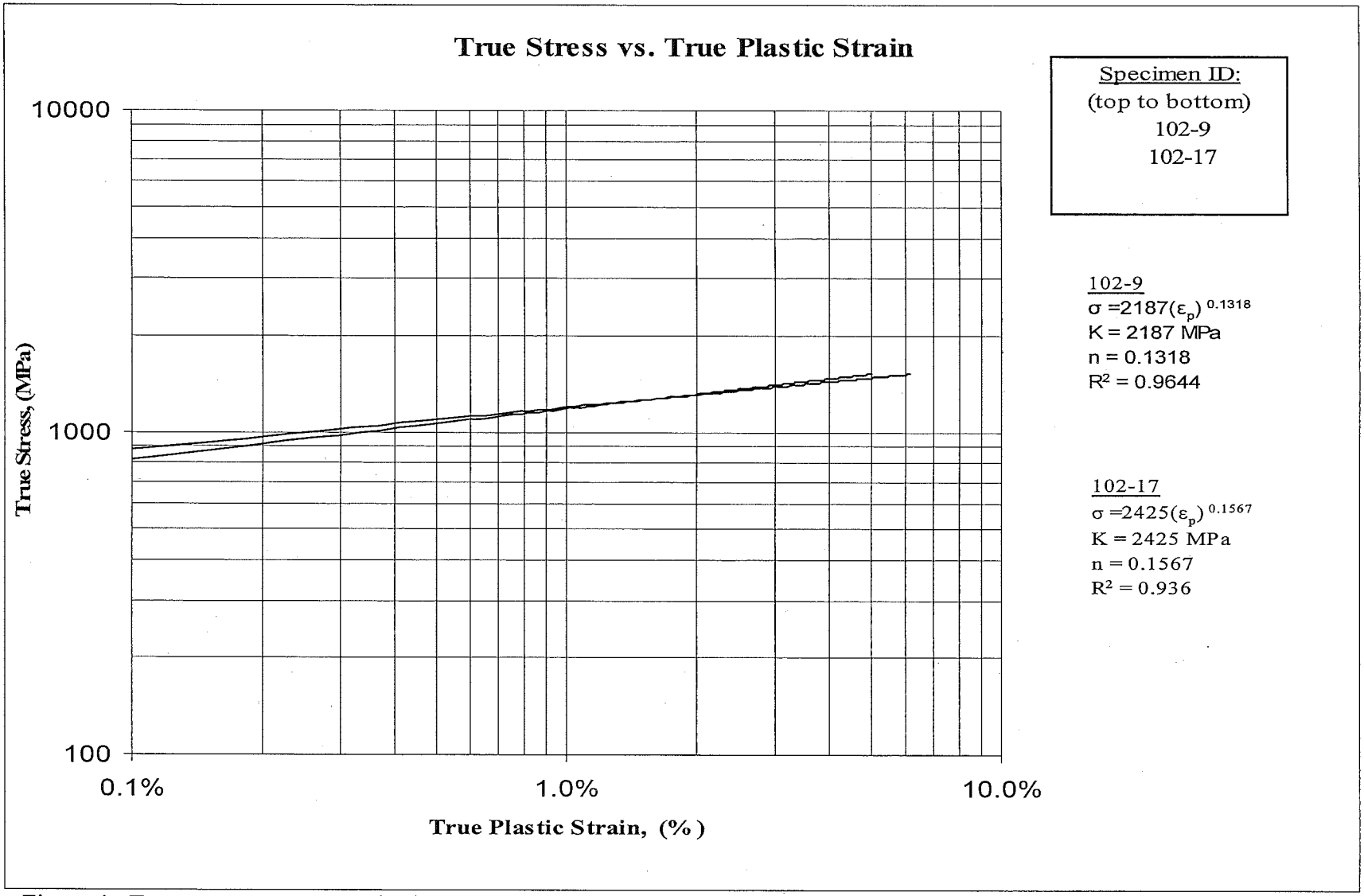

Figure 4: True stress versus true plastic strain

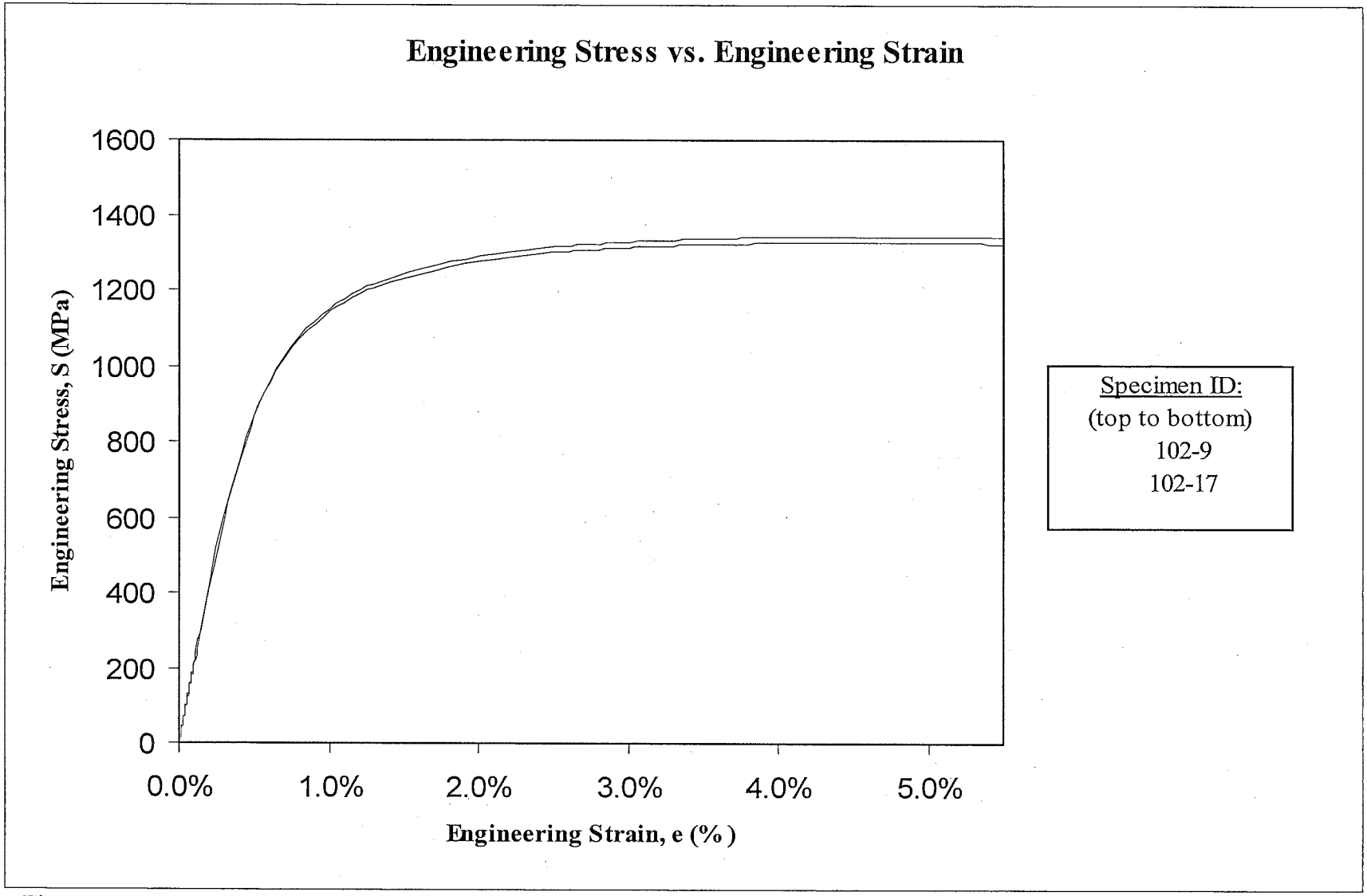

Figure 5: Monotonic stress-strain curves

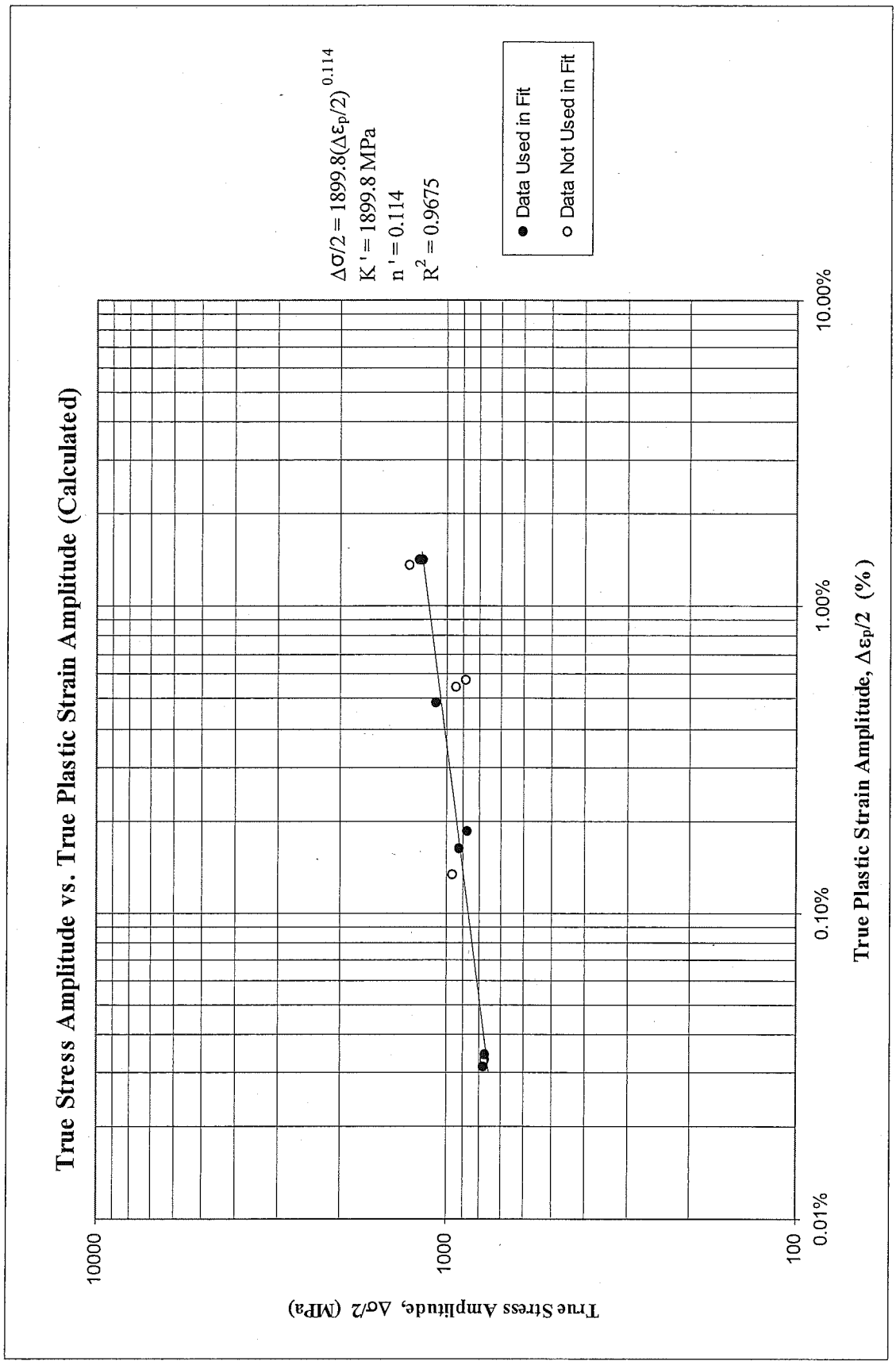

Figure 6: True stress amplitude versus true plastic strain amplitude (calculated)

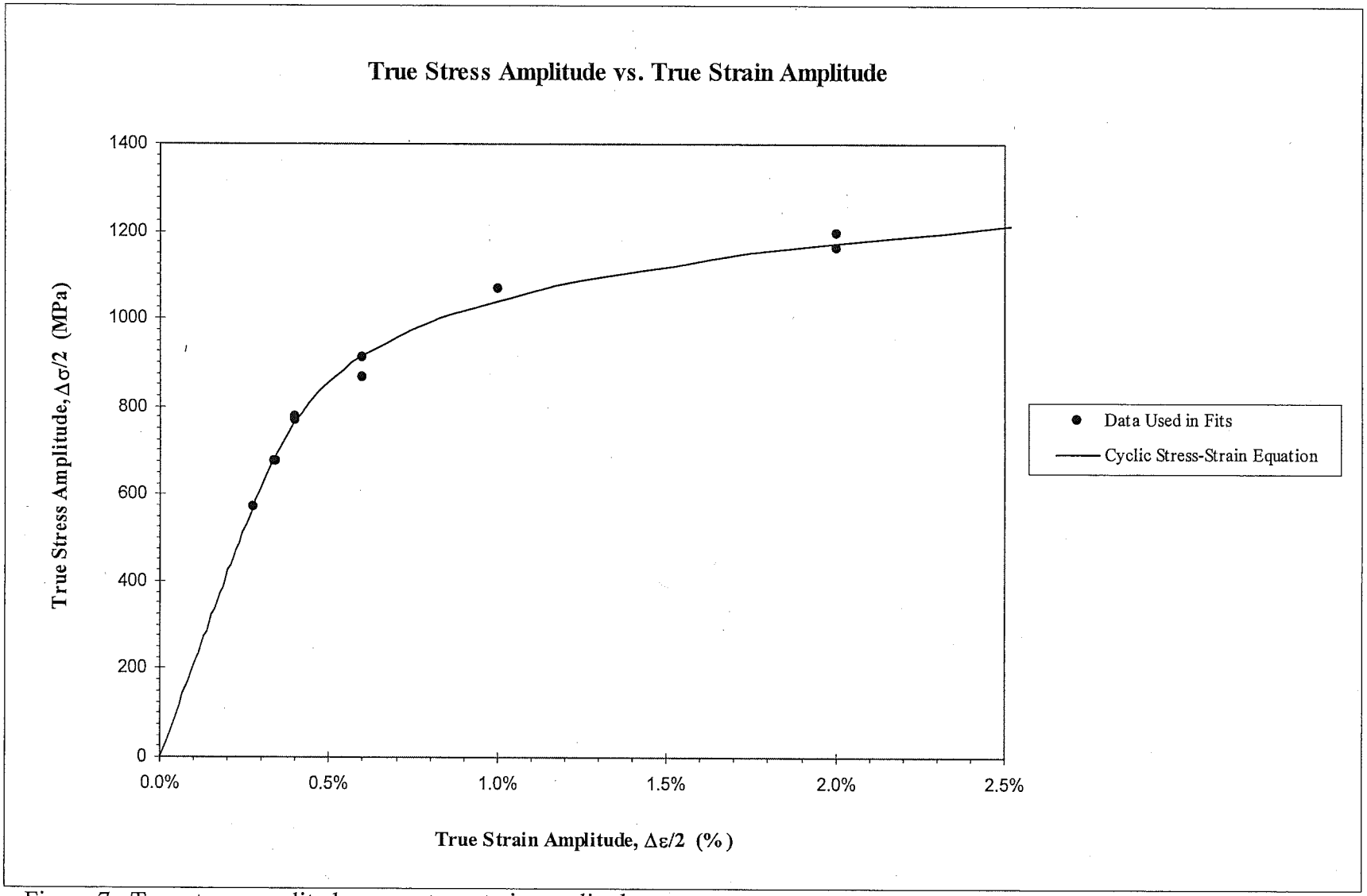

Figure 7: True stress amplitude versus true strain amplitude

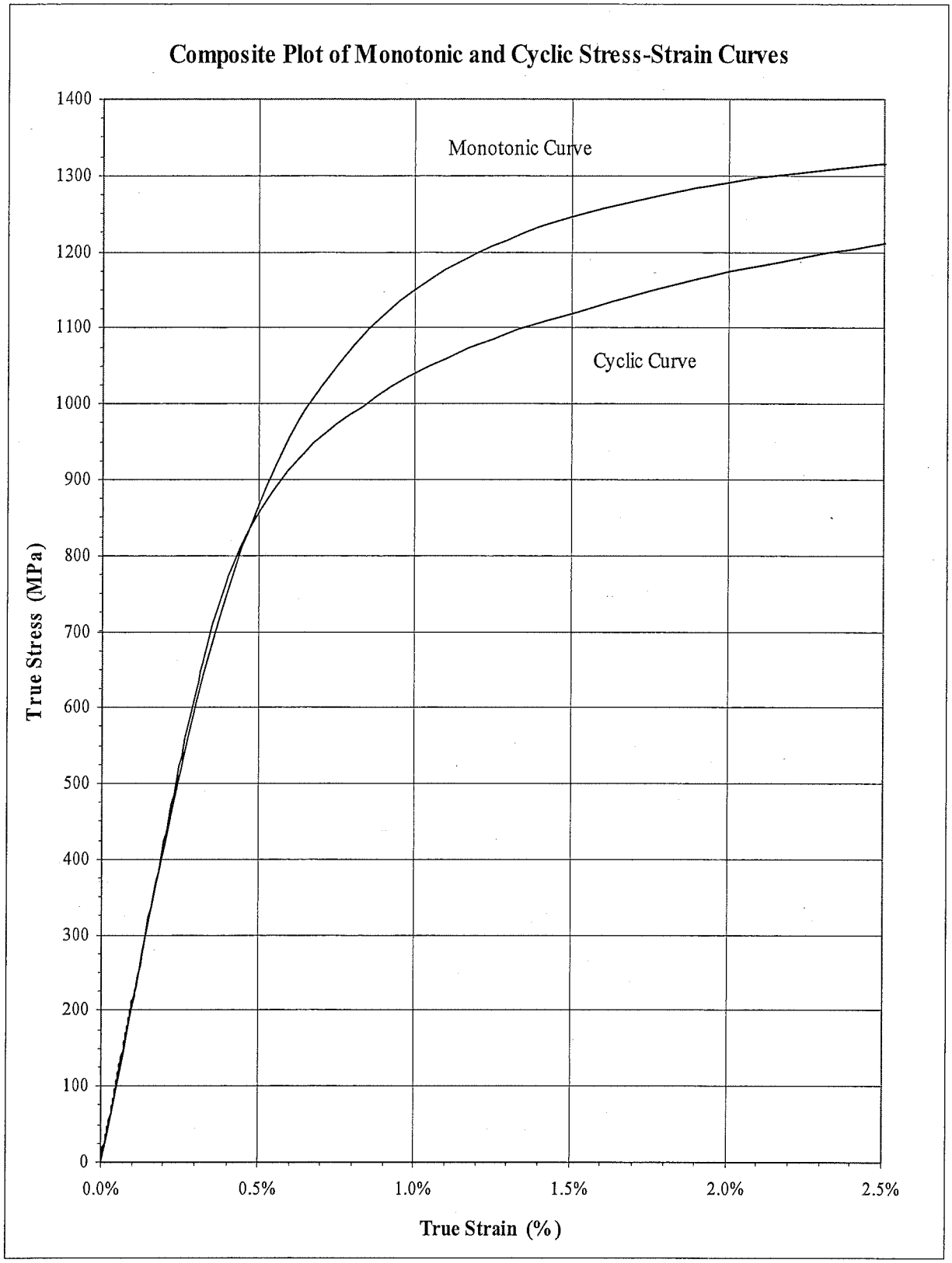

Figure 8: Composite plot of cyclic and monotonic stress-strain curves

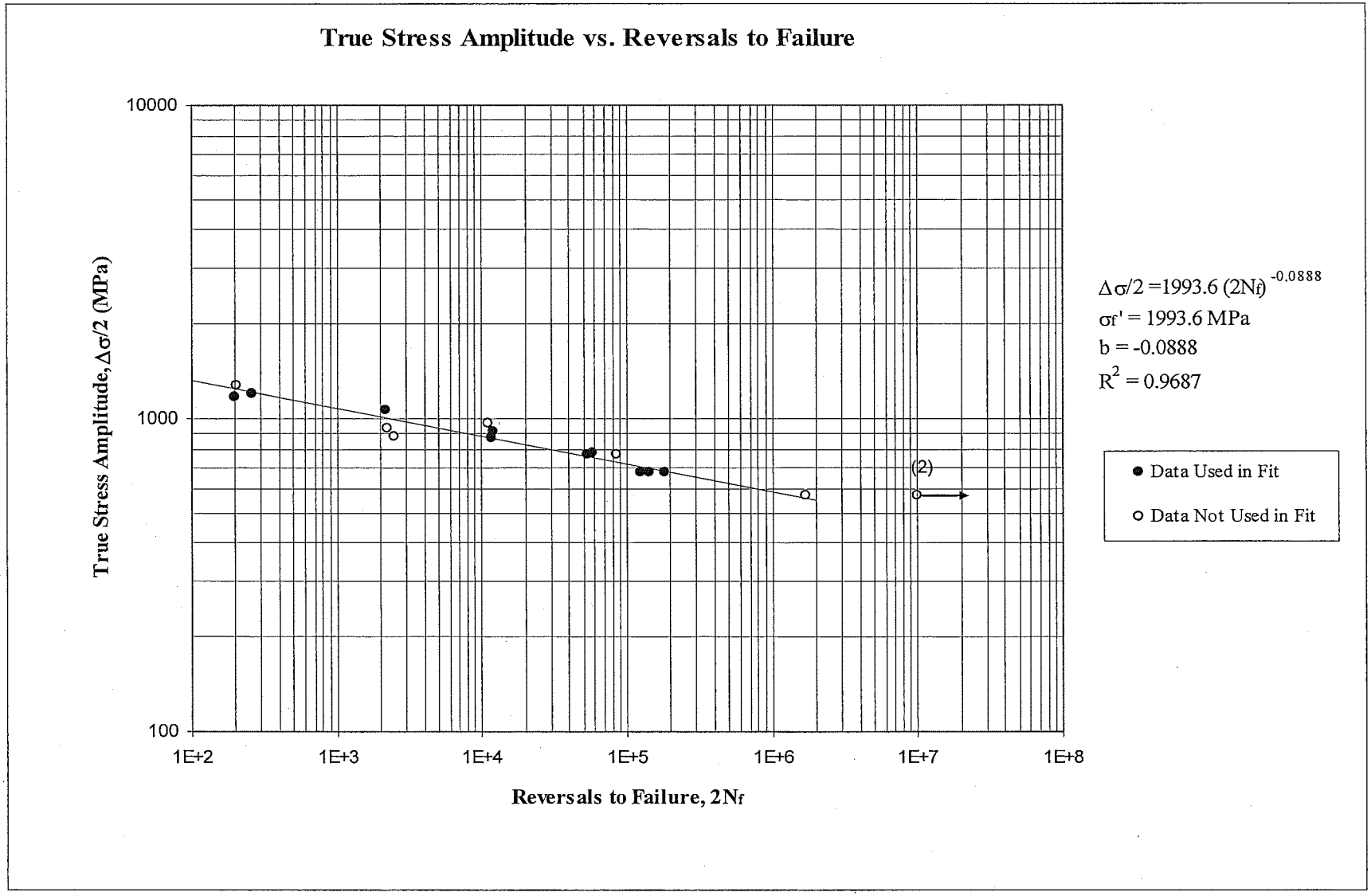

Figure 9: True stress amplitude versus reversals to failure

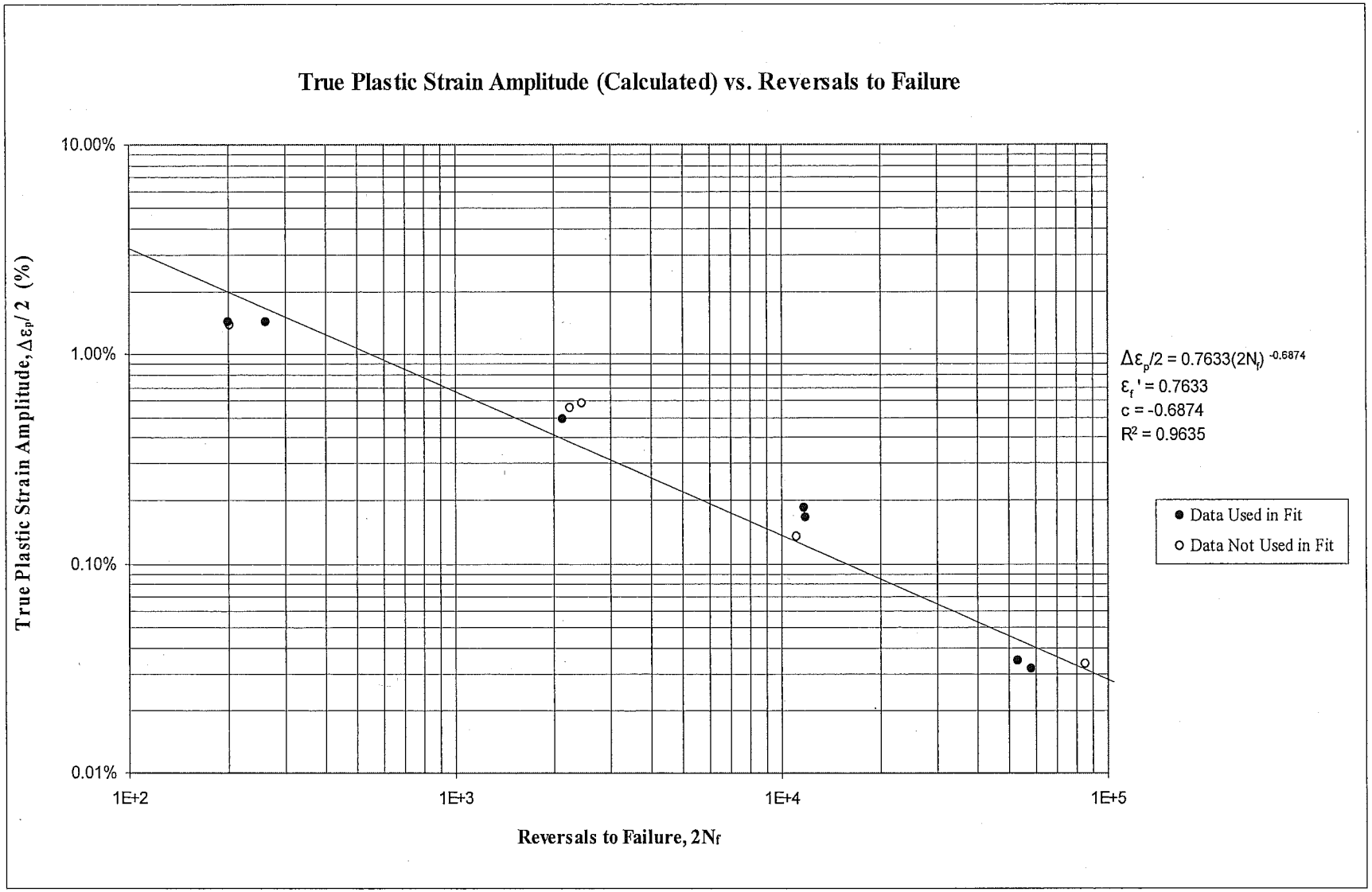

Figure 10: True plastic strain amplitude (calculated) versus reversals to failure

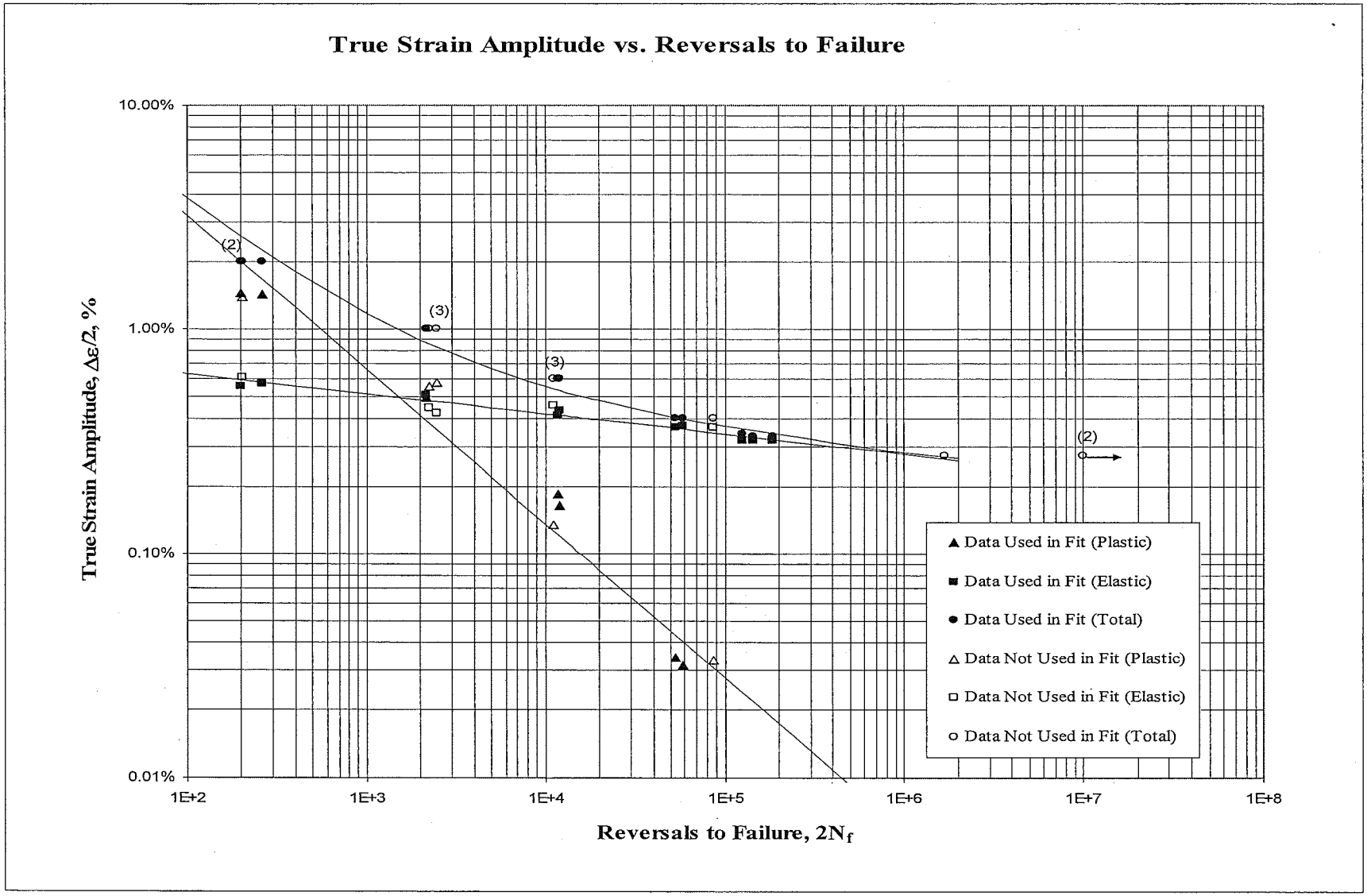

Figure 11: True strain amplitude versus reversals to failure

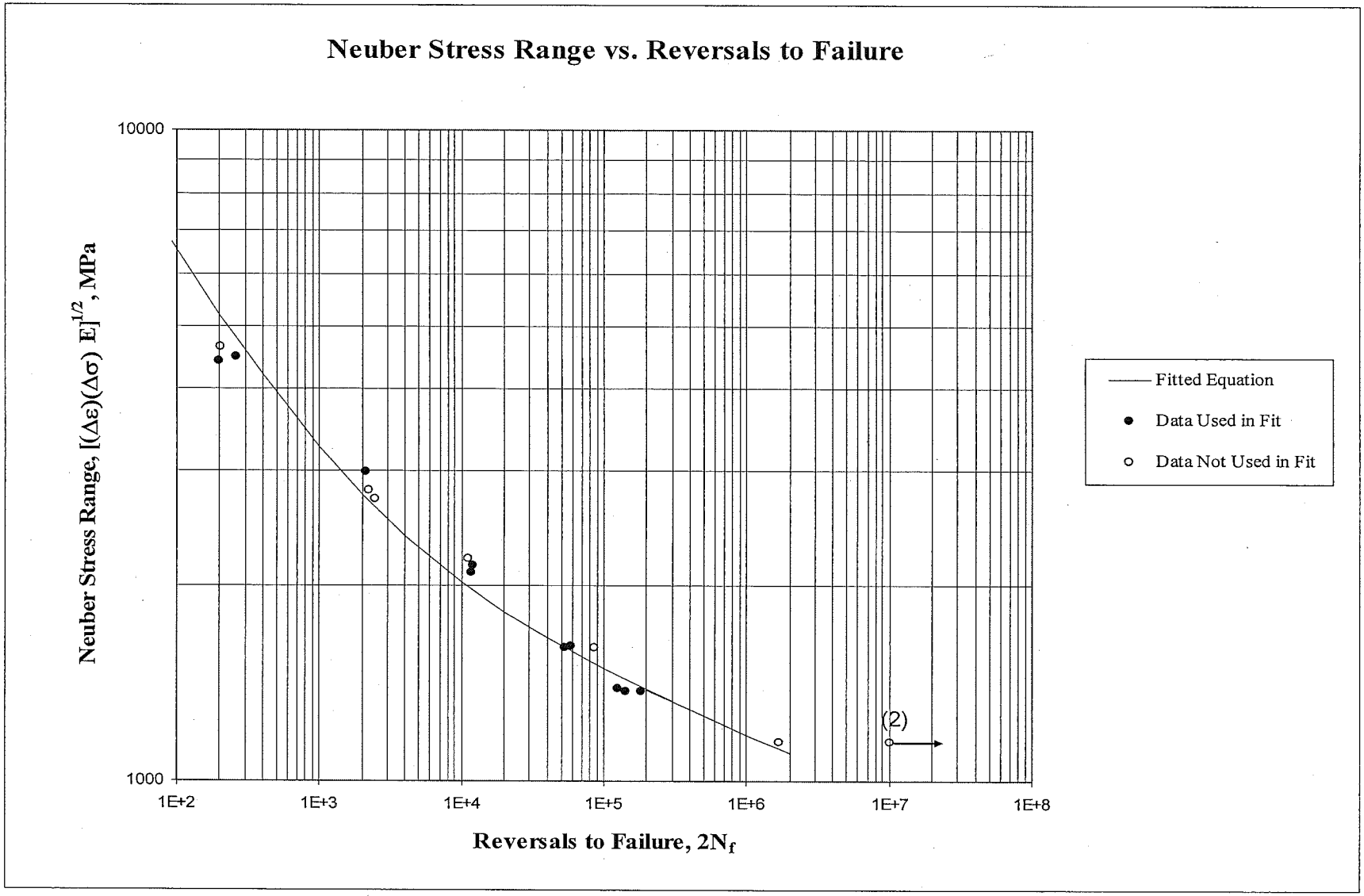

Figure 12: Neuber stress range versus reversals to failure

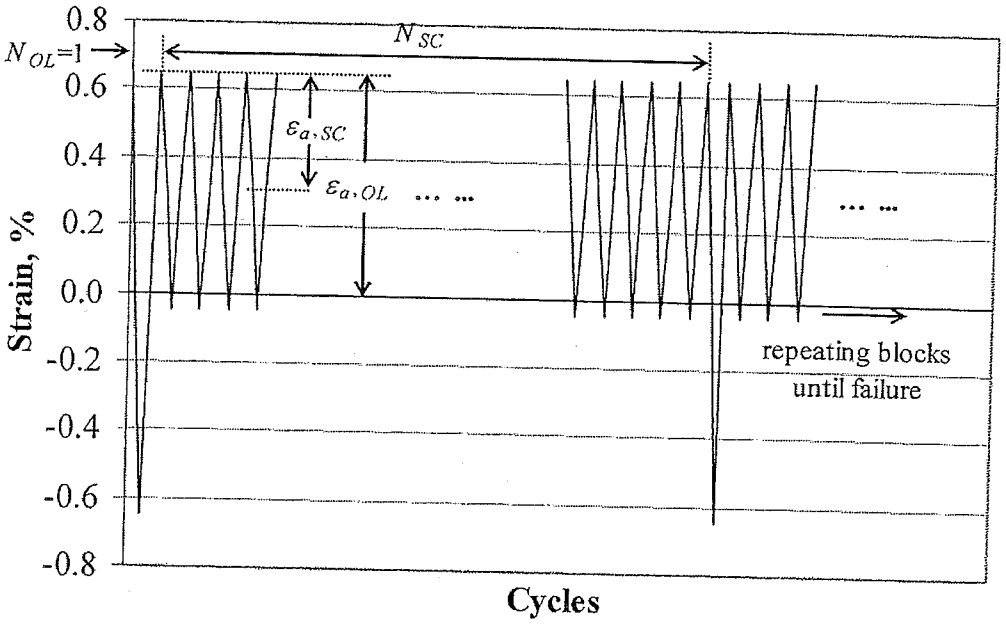

Figure 13: Periodic overload history

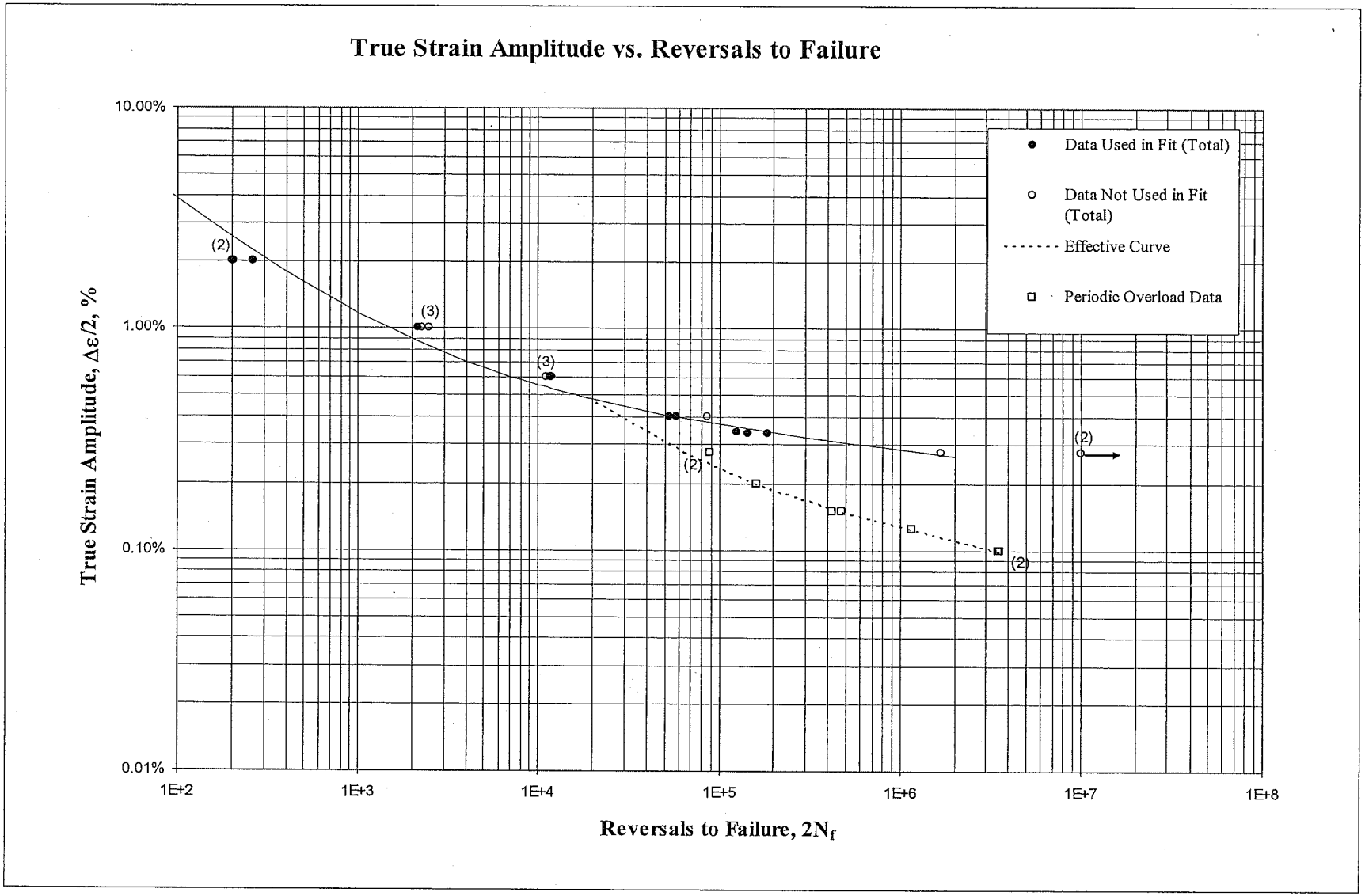

Figure 14: Periodic overload data superimposed with constant amplitude fatigue data

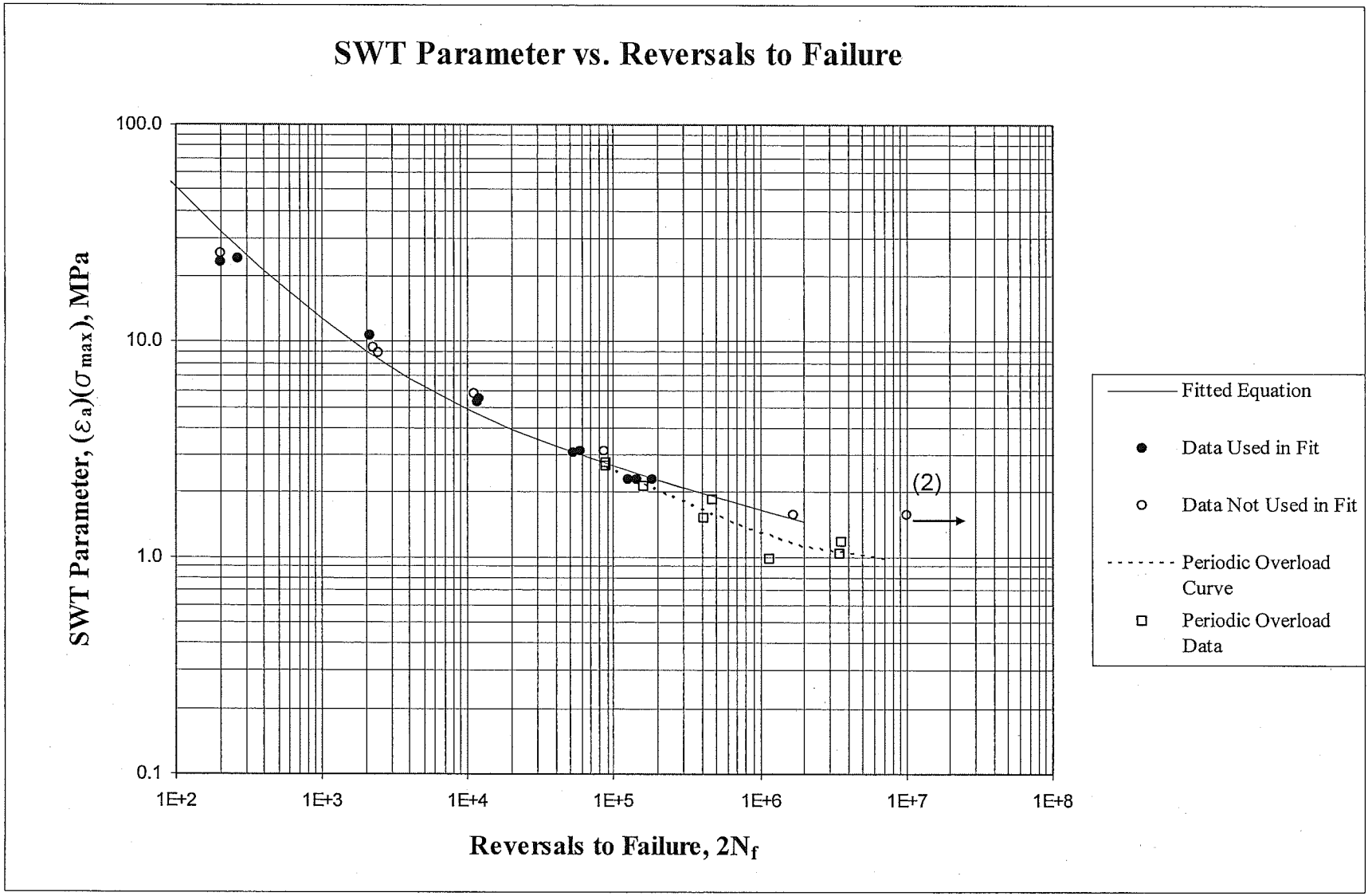

Figure 15: SWT parameter versus reversals to failure. Periodic overload data superimposed on constant amplitude data

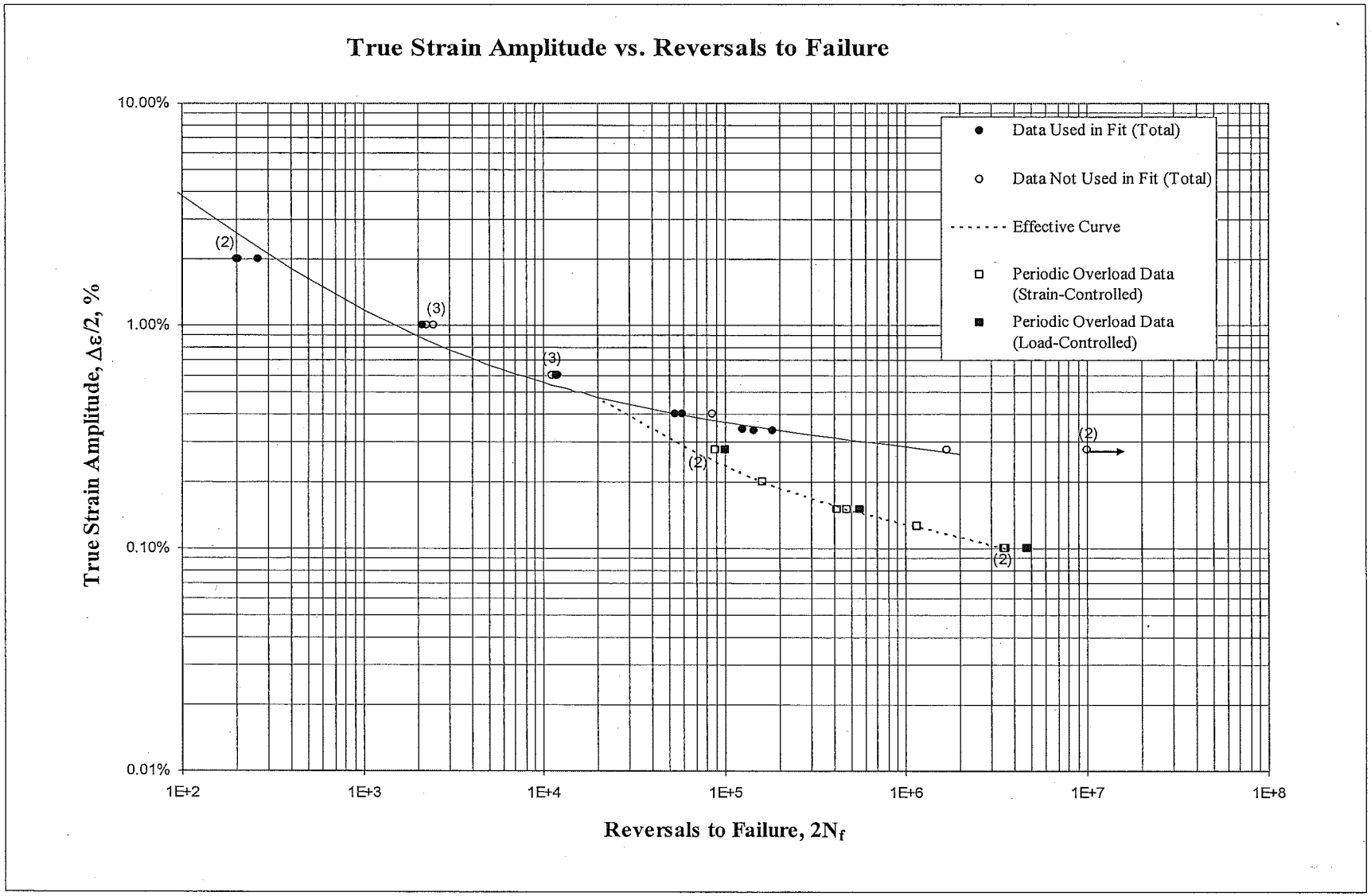

Figure 16: Load controlled Periodic overload data superimposed with strain controlled fatigue data

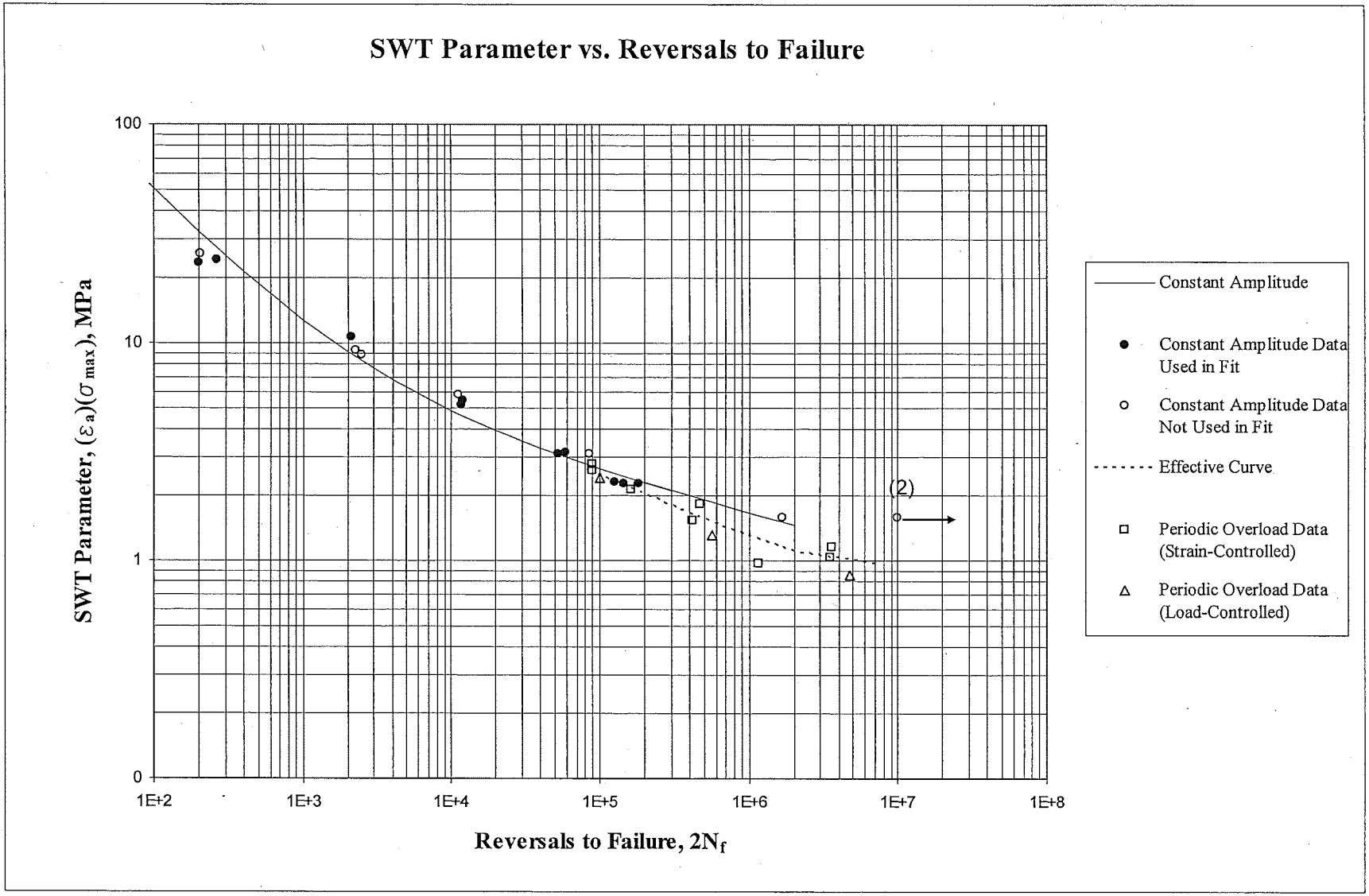

Figure 17: SWT Parameter. Load controlled Periodic overload data superimposed with strain controlled fatigue data

REFERENCES

[1] ASTM Standard E606-92, "Standard Practice for Strain-Controlled Fatigue Testing," Annual Book of ASTM Standards, Vol. 03.01, 2004, pp. 593-606.

[2] ASTM Standard E83-02, "Standard Practice for Verification and Classification of Extensometers," Annual Book of ASTM Standards, Vol. 03.01, 2004, pp. 232-244.

[3] ASTM Standard E1012-99, "Standard Practice for Verification of Specimen Alignment Under Tensile Loading," Annual Book of ASTM Standards, Vol. 03.01, 2004, pp. 763-770.

[4] ASTM Standard E8-04, "Standard Test Methods for Tension Testing of Metallic Materials," Annual Book of ASTM Standards, Vol. 03.01, 2004, pp. 62-85.

[5] ASTM Standard E739-91, "Standard Practice for Statistical Analysis of Linear or Linearized Stress-Life (S-N) and Strain-Life (ε-N) Fatigue Data," Annual Book of ASTM Standards, Vol. 03.01, 1995, pp. 670-676.

[6] ASTM Standard E646-00, "Standard Test Method for Tensile Strain-Hardening Exponents (n-values) of Metallic Sheet Materials," Annual Book of ASTM Standards, Vol. 03.01, 2004, pp. 619-626.

[7] Stephens R. I., Fatemi A., Stephens R. R. and Fuchs H. O., "*Metal Fatigue in Engineering*", Second edition, Wiley Interscience, 2000.

Appendix A

Table A.1: Summary of monotonic tensile test results

Specimen ID	D_o, mm (in)	D_f, mm (in)	L_o, mm (in)	L_f, mm (in)	E, Gpa (ksi)	YS (offset=0.2%), Mpa (ksi)	UYS, Mpa	LYS, Mpa	YPE, Mpa	S_u, Mpa (ksi)	K, Mpa (ksi)	n	%EL	%RA	R, mm (in)	σ_f, Mpa (ksi)	ε_f, %
102-17	4.801 (0.1890)	3.518 (0.1385)	7.620 (0.3000)	9.40 (0.3701)	210.5 (30,524)	990 (143.6)	-	-	-	1326.1 (192.3)	2424.5 (351.6)	0.1567	23.4%	46.3%	1.969 (0.0775)	1521.9 (220.7)	62.2%
102-9	4.801 (0.1890)	3.480 (0.1370)	7.620 (0.3000)	9.47 (0.3728)	209.5 (30,391)	990 (143.6)	-	-	-	1343.4 (194.8)	2186.9 (317.2)	0.1318	24.3%	47.5%	2.032 (0.0800)	1562.6 (226.6)	64.4%
Average Values					210.0 (30,457)	990 (143.6)	-	-	-	1334.7 (193.6)	2305.7 (334.4)	0.1443	23.8%	46.9%	2.000 (0.0788)	1542.3 (223.7)	63.3%

Table A.2: Summary of constant amplitude completely reversed fatigue test results

Specimen ID	Test control mode	Test freq., Hz	E, GPa (ksi) [e]	At midlife ($N_{50\%}$)							$(2N_f)_{10\%}$, [b] reversals	$(2N_f)_{50\%}$, [c] reversals	Failure location [d]
				E', GPa (ksi)	$\Delta\varepsilon/2$, %	$\Delta\varepsilon_p/2$ (calculated), %	$\Delta\varepsilon_p/2$ (measured), %	$\Delta\sigma/2$, MPa (ksi)	σ_m, MPa (ksi)	$2N_{50\%}$, [a] reversals			
102-4	strain	0.2	209.2 (30,341)	200.6 (29,086)	1.988%	1.435%	1.390%	1162.0 (168.5)	-2.4 (-0.3)	128	198	200	IGL
102-3*	strain	0.2	206.5 (29,949)	-	1.989%	1.382%	-	1273.5 (184.7)	-6.8 (-1.0)	128	-	204	IGL
102-5	strain	0.2	209.6 (30,399)	201.7 (29,253)	1.997%	1.428%	1.355%	1194.6 (173.3)	-5.1 (-0.7)	128	260	262	IGL
102-8	strain	0.3	209.5 (30,384)	198.9 (28,840)	0.999%	0.491%	0.430%	1066.4 (154.7)	-16.0 (-2.3)	1,024	-	2,134	IGL
102-2*	strain	0.3	210.5 (30,529)	-	0.996%	0.552%	-	931.6 (135.1)	-5.8 (-0.8)	1,024	-	2,248	IGL
102-1*	strain	0.3	208.5 (30,239)	-	0.999%	0.579%	-	881.4 (127.8)	-9.7 (-1.4)	1,024	-	2,456	IGL
102-20*	strain	1.0	212.2 (3,078)	-	0.600%	0.135%	-	961.7 (139.5)	23.6 (3.4)	4,096	11,058	11,062	IGL
102-7	strain	1.0	207.7 (30,123)	201.3 (29,195)	0.599%	0.186%	0.175%	867.6 (125.8)	19.5 (2.8)	4,096	11,680	11,688	IGL
102-10	strain	1.0	208.4 (30,249)	205.0 (29,755)	0.598%	0.164%	0.138%	911.4 (132.2)	7.0 (1.0)	4,096	11,646	11,892	IGL
102-15	strain load	5.0 5.0	206.4 (29,935)	203.2 (29,463)	0.402%	0.034%	0.026%	771.1 (0.0)	0.0 (0.0)	-	-	52,936	IGL
102-6	strain load	5.0 5.0	207.1 (30,036)	205.0 (29,732)	0.400%	0.032%	0.025%	772.6 (111.7)	0.0 (0.0)	-	-	58,530	IGL
102-12*	strain load	5.0 5.0	210.1 (30,471)	-	0.400%	0.033%	-	770.3 (112.1)	0.0 (0.0)	-	-	85,650	IGL
102-16	load	10	-	-	0.340%	-	-	676.0 (98.0)	0.0 (0.0)	-	-	125,466	IGL
102-19	load	10	-	-	0.335%	-	-	676.0 (98.0)	0.0 (0.0)	-	-	144,000	IGL
102-14	load	10	-	-	0.335%	-	-	676.0 (98.0)	0.0 (0.0)	-	-	184,000	IGL
102-21	load	24	-	-	0.275%	-	-	572.0 (83.0)	0.0 (0.0)	-	-	845,868	IGL
102-11	load	24	-	-	0.275%	-	-	572.0 (17.8)	0.0 (0.0)	-	-	>10,000,000	No Failure
102-18	load	24	-	-	0.275%	-	-	572.0 (17.8)	0.0 (0.0)	-	-	>10,000,000	No Failure

* Data from this test was not used in fits due to large measured hardness variation

[a] $2N_{50\%}$ is defined as the midlife reversal ; [b] $2(N_f)_{10\%}$ is defined as reversal of 10% load drop

[c] $2(N_f)_{50\%}$ is defined as reversal of 50% load drop or failure

[d] IGL = Inside gage length

[e] E value was calculated from the first cycle

Table A.3: Summary of the periodic overload fatigue test results

Spec. ID	Test Control Mode	Test Freq. OL/SC (Hz)	E (GPa) [b]	Load history Description												Exp. Life (Blks)	$N_{f,sc(eq)}$ (Cycles)	OL Damage Ratio	Failure Location [a]
				$\varepsilon_{a,SC}$ (%)	$\varepsilon_{m,SC}$ (%)	$\Delta\varepsilon_p/2_{,SC}$ (calculated) (%)	$\sigma_{a,SC}$ (MPa)	$\sigma_{m,SC}$ (MPa)	N_{SC} (Cycles)	$\varepsilon_{a,OL}$ (%)	$\Delta\varepsilon_p/2_{,OL}$ (calculated) (%)	$\sigma_{a,OL}$ (MPa)	$\sigma_{m,OL}$ (MPa)	$N_{f,OL}$ (Cycles)				
106_06	Strain	1 / 3	208.3	0.270%	0.206%	0.008%	544.9	424.9	30	0.475%	0.046%	894.3	77.4	10,190	1,299	44,664	0.127	IGL
102_25	Strain	1 / 4	202.5	0.265%	0.198%	0.003%	530.2	508.3	30	0.463%	0.033%	871.2	170.0	10,190	1,298	44,624	0.127	IGL
106_09	Load	1 / 3	204.8	0.285%	0.157%	0.004%	575.6	265.4	30	0.442%	0.033%	838.3	2.3	10,190	1,301	50,414	0.228	IGL
102_22	Strain	1 / 4	207.2	0.200%	0.270%	0.003%	406.6	662.5	100	0.470%	0.060%	849.2	216.4	10,190	748	80,726	0.073	IGL
106_02	Strain	1 / 7	206.4	0.150%	0.314%	0.004%	302.5	914.4	200	0.464%	0.049%	856.6	358.3	10,190	1,059	236,364	0.104	IGL
102_23	Strain	1 / 7	204.8	0.150%	0.315%	0.002%	302.9	710.0	200	0.465%	0.064%	821.5	189.6	10,190	949	209,291	0.093	IGL
106_05	Load	1 / 7	205.6	0.155%	0.283%	0.001%	316.9	522.3	200	0.438%	0.034%	830.9	7.0	10,190	1,113	280,834	0.209	IGL
102_30	Strain	1 / 7	203.5	0.125%	0.339%	0.001%	252.7	526.8	300	0.464%	0.040%	861.8	-81.5	10,190	1,630	582,116	0.160	IGL
102_27	Strain	1 / 7	207.2	0.100%	0.365%	0.002%	203.4	832.5	1,000	0.465%	0.064%	831.3	204.1	10,190	1,505	1,765,797	0.148	IGL
102_24	Strain	1 / 7	205.0	0.100%	0.365%	0.002%	199.8	961.2	1,000	0.464%	0.056%	836.6	322.8	10,190	1,513	1,776,820	0.148	IGL
106_12	Load	1 / 7	205.2	0.101%	0.337%	-0.002%	211.3	626.1	1,000	0.439%	0.028%	842.2	1.3	10,190	1,725	2,354,689	0.269	IGL

[a] IGL = Inside gage length

[b] E value was calculated from the first cycle

All stress values reported are from mid-life

Load-controlled tests were pre-cycled at the OL stress amplitude for 1000 cycles. Damage from the pre-strained cycles is included in the OL damage ratio

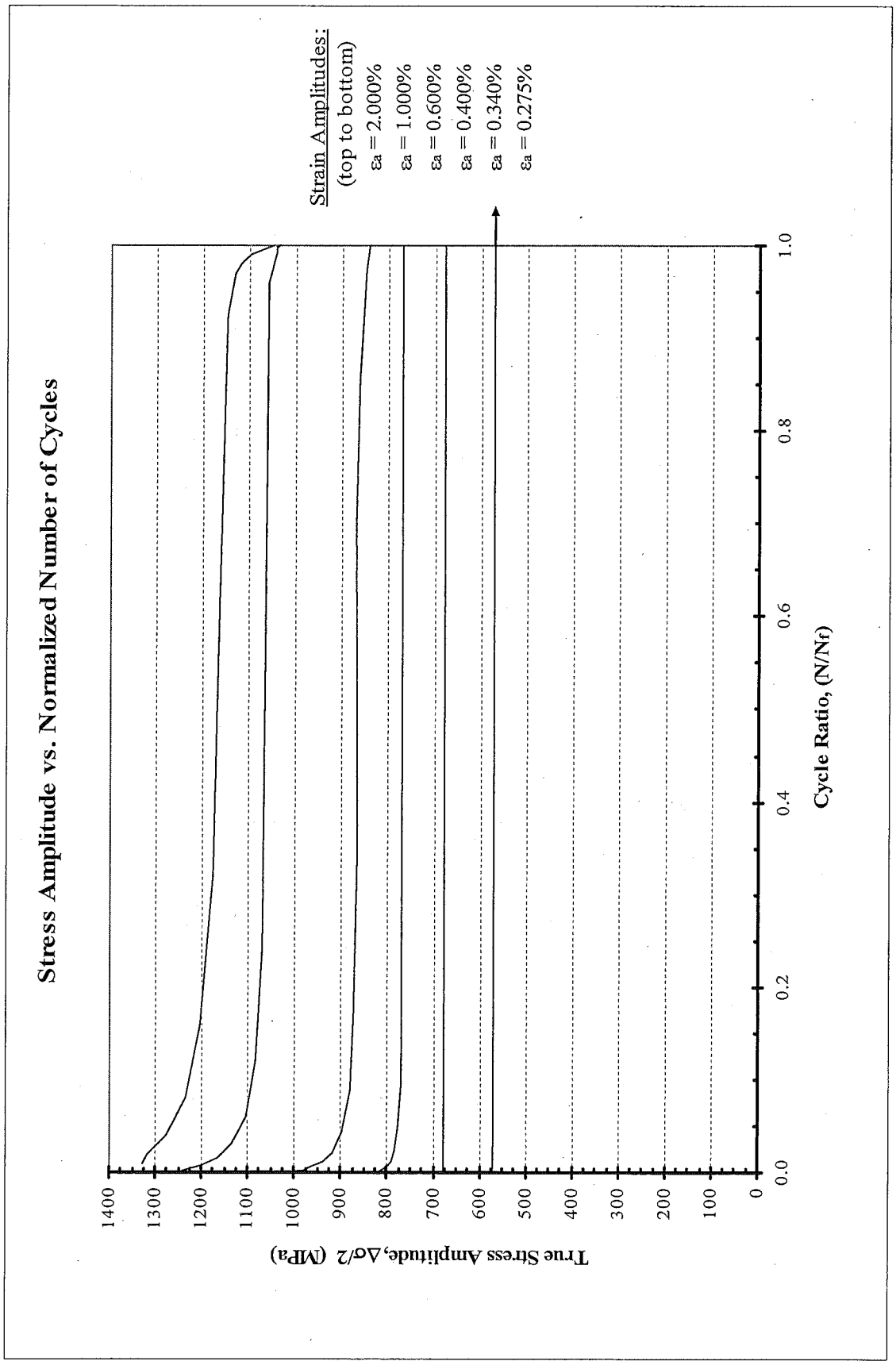

Figure A.1a: True stress amplitude versus normalized number of cycles

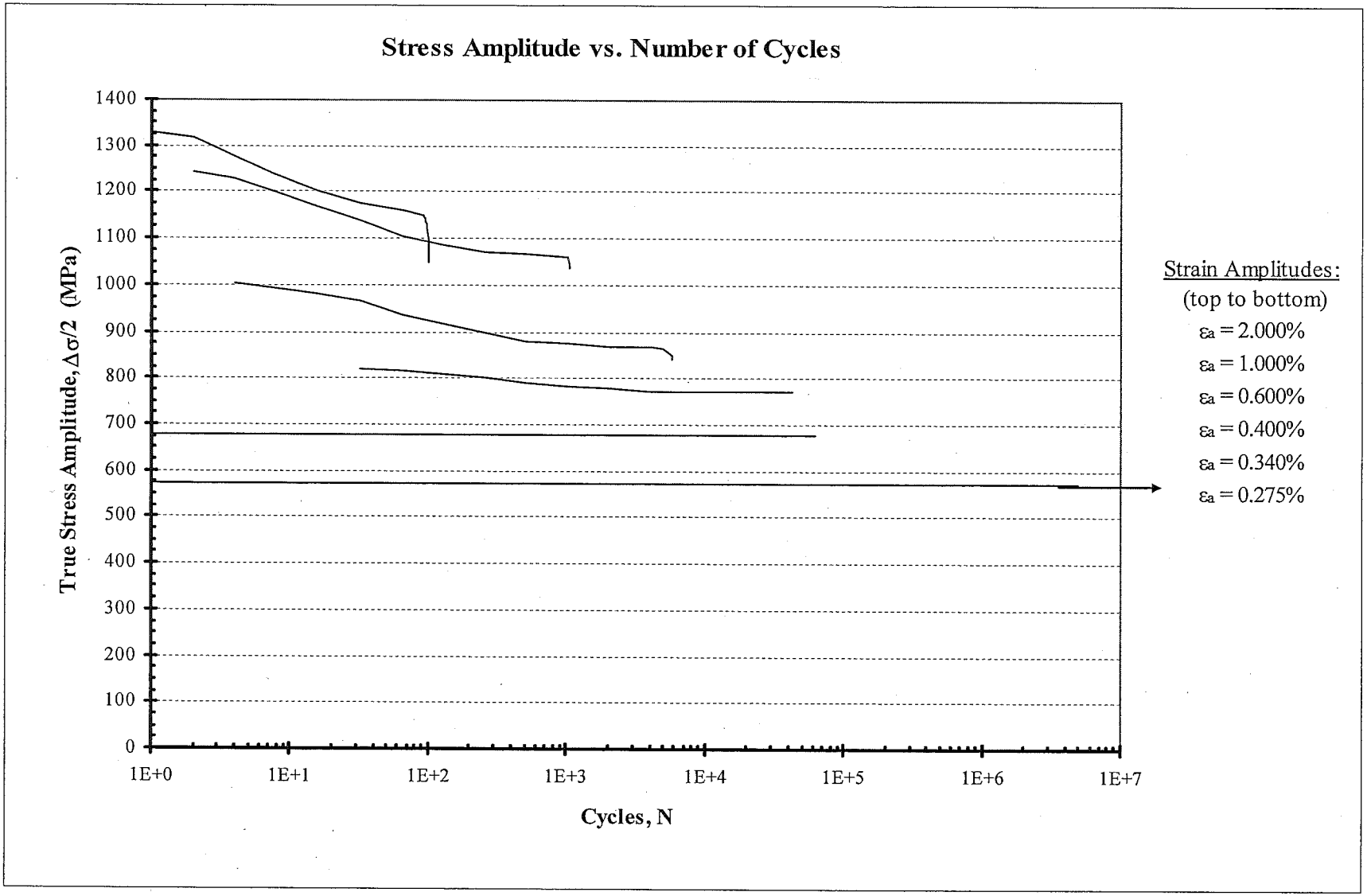

Figure A.1b: True stress amplitude versus number of cycles

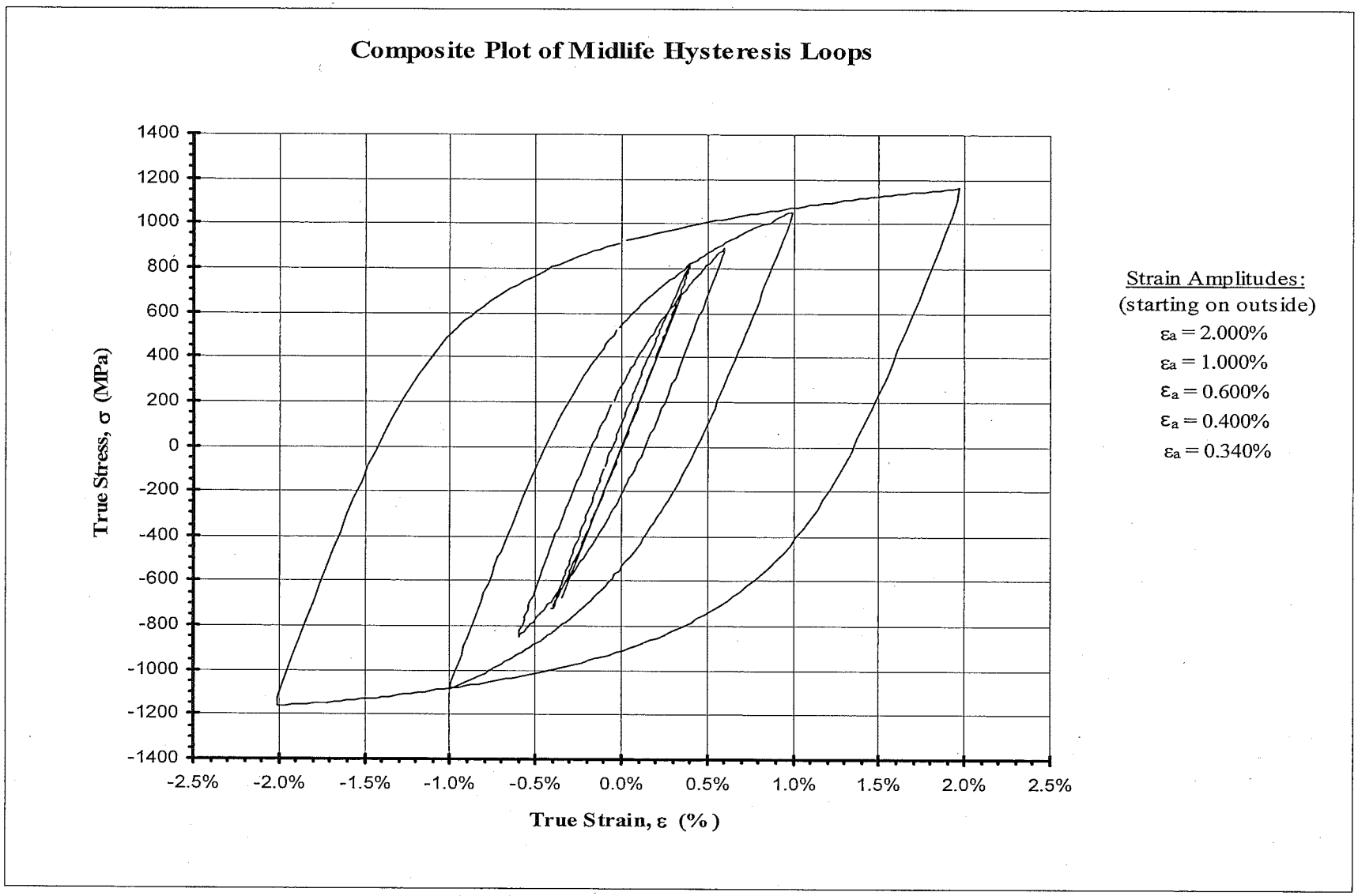

Figure A.2: Composite plot of midlife hysteresis loops

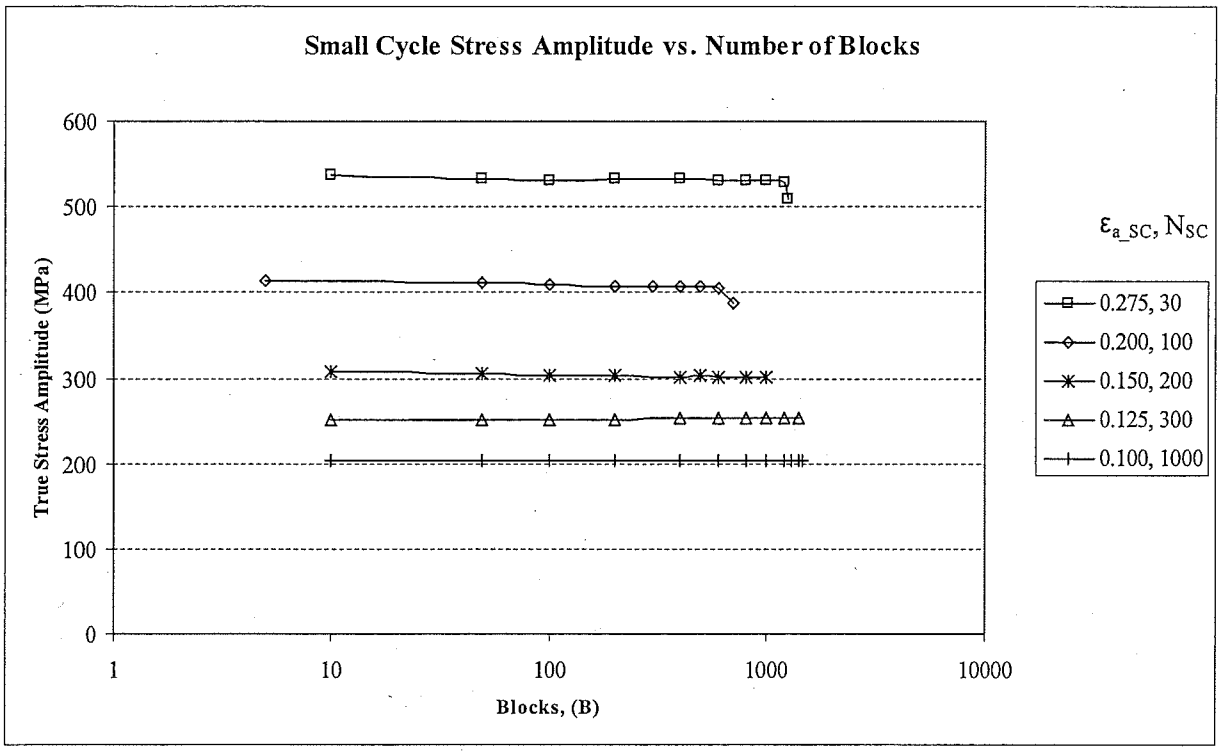

Figure A.3a: Small cycle amplitude transient response throughout the life.

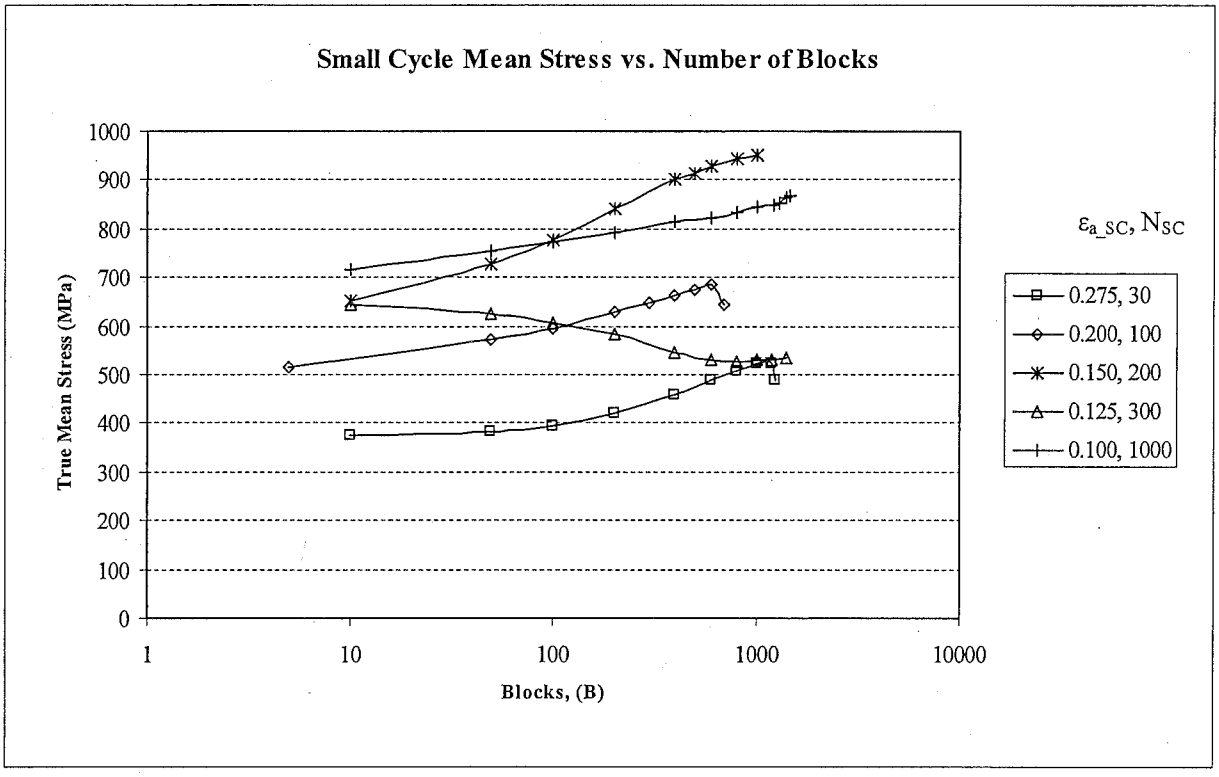

Figure A.3b: Small cycle mean transient response throughout the life.

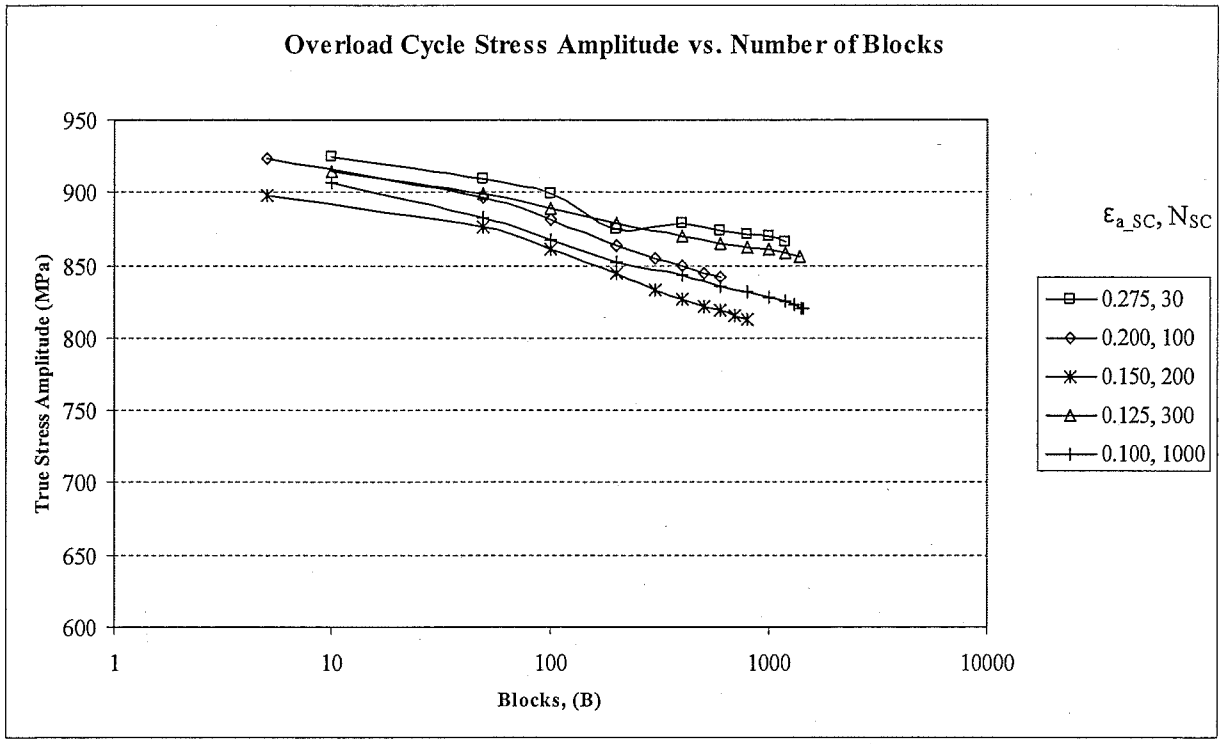

Figure A.4a: Overload cycle amplitude transient response throughout the life.

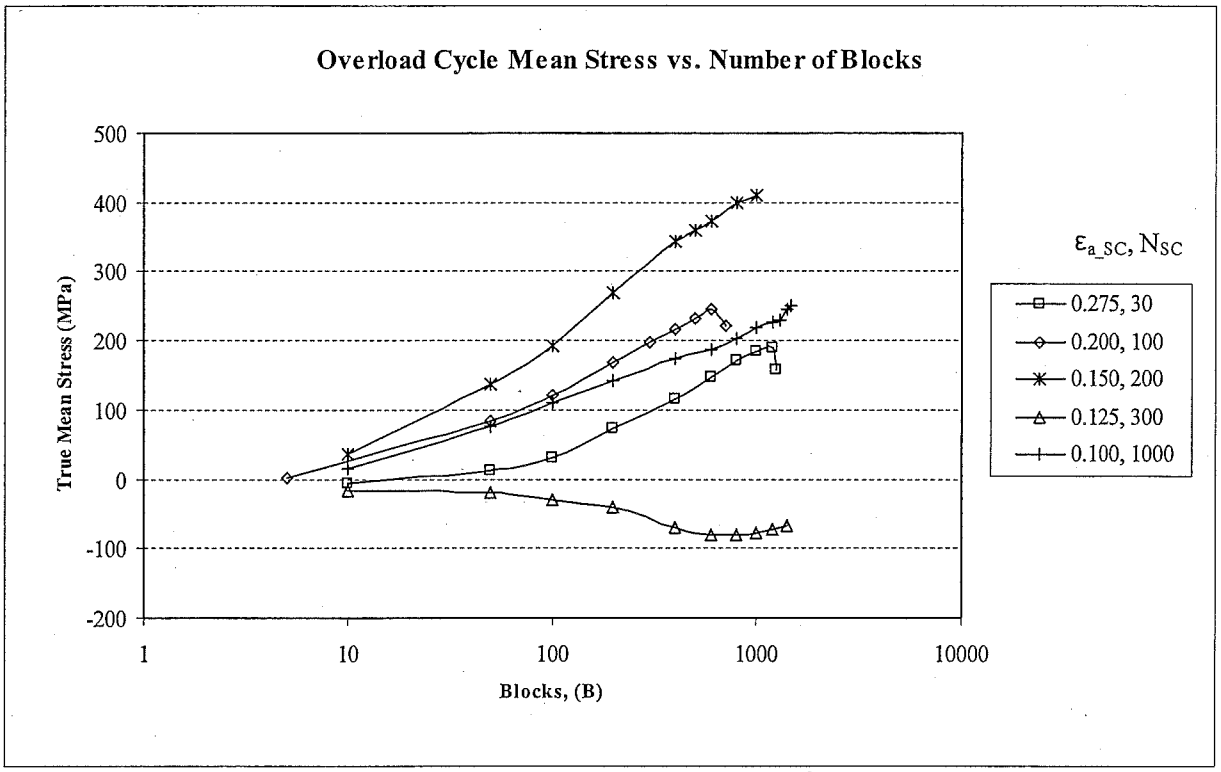

Figure A.4b: Overload cycle mean transient response throughout the life.

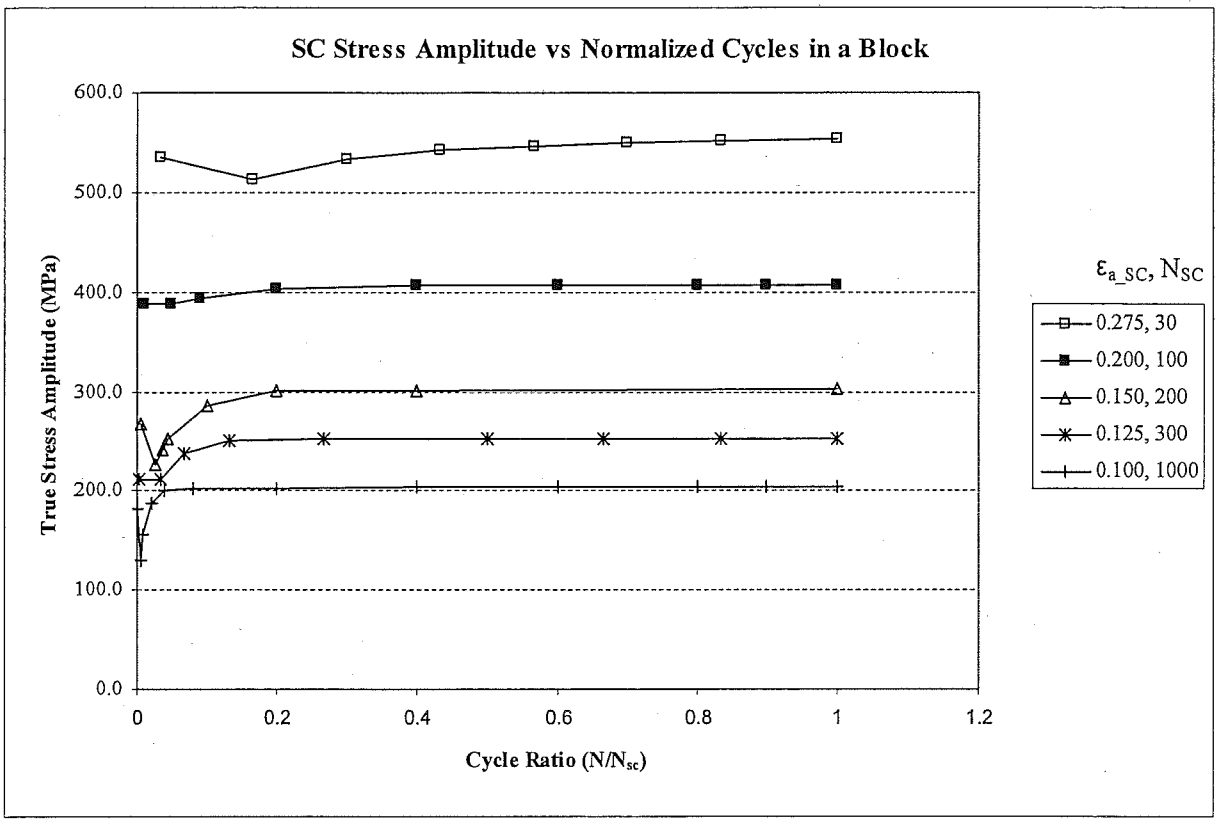

Figure A.5a: Small cycle transient response amplitude throughout one load block at midlife.

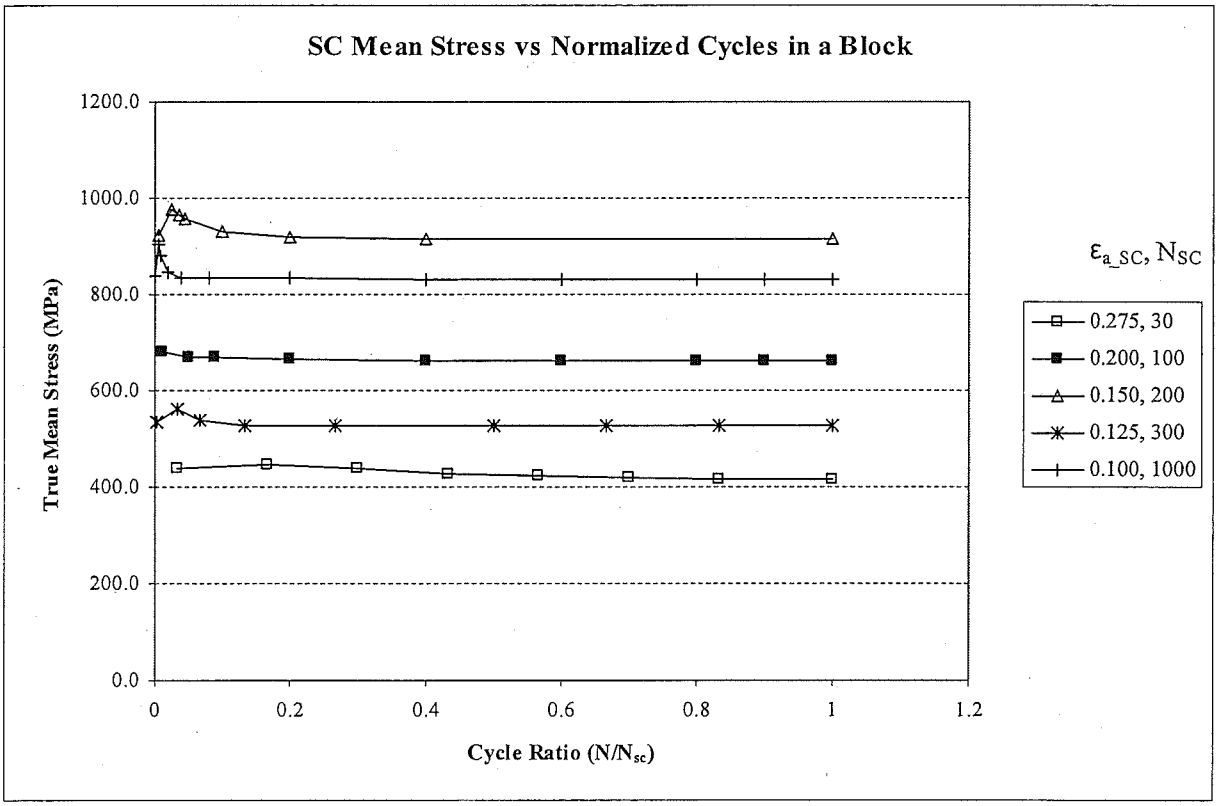

Figure A.5b: Small cycle transient response mean throughout one load block at midlife.

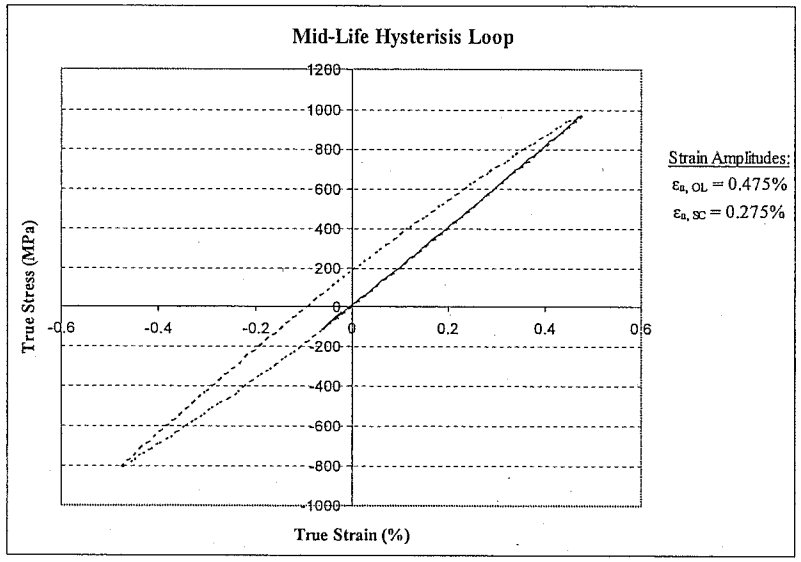

(a)

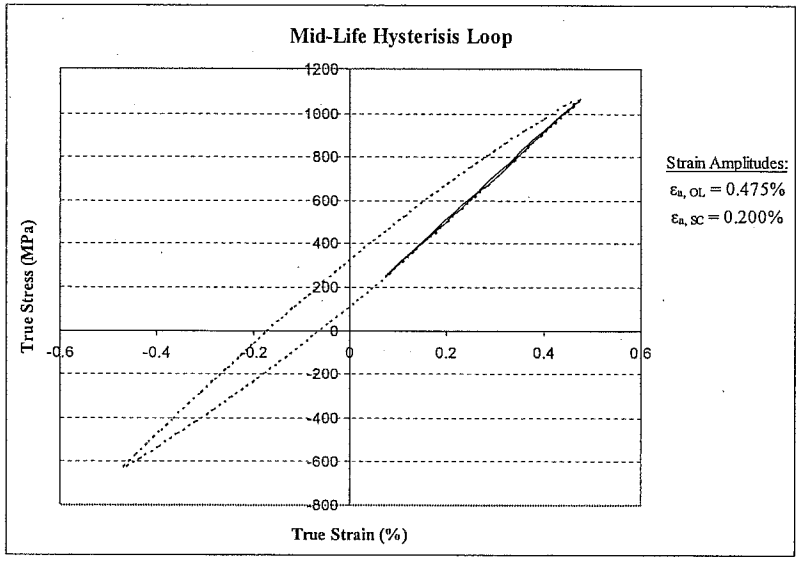

(b)

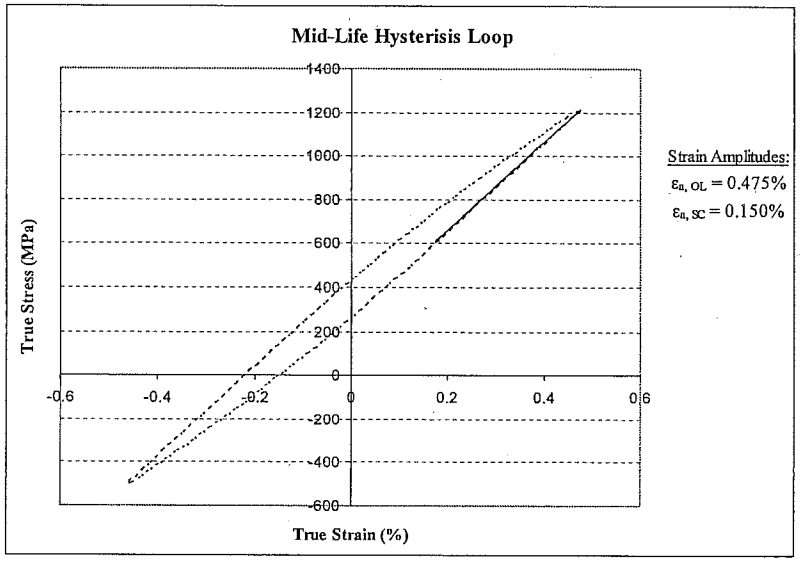

(c)

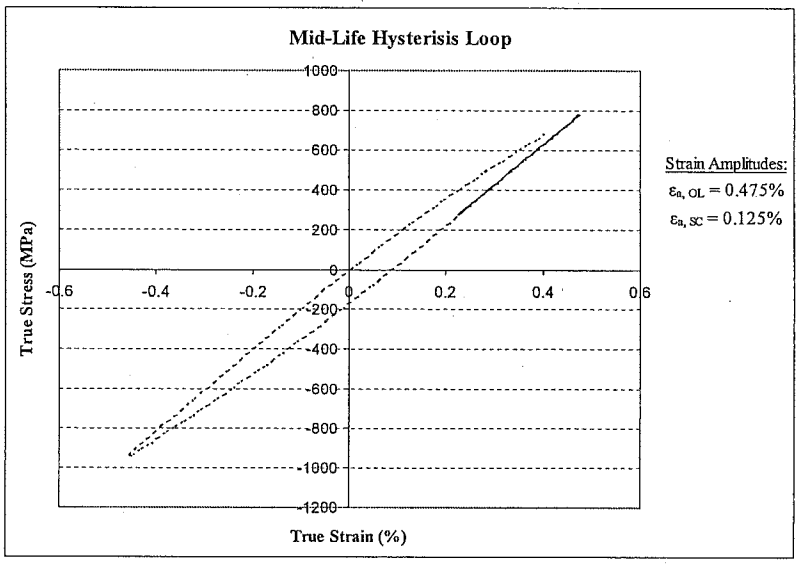

(d)

Figure A.6(a-e): Periodic overload midlife hysterisis loop superimposed with small cycle midlife hysterisis loop

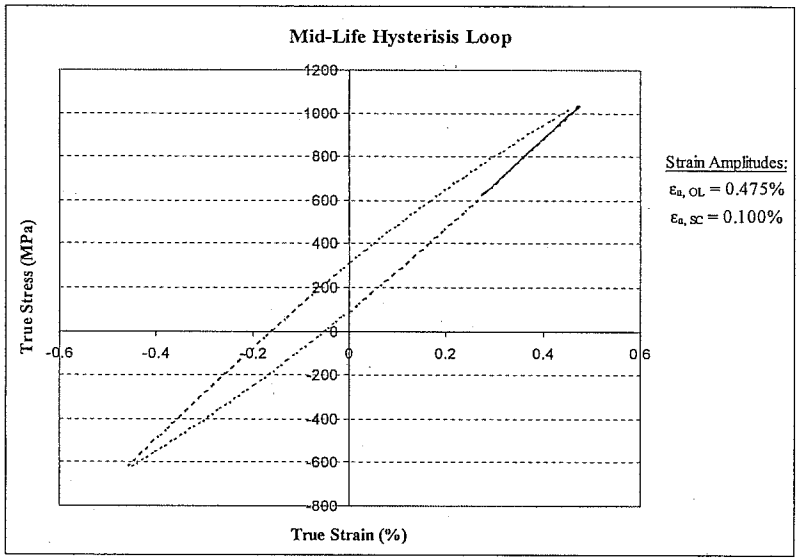

(e)

Figure A.6(a-e): Periodic overload midlife hysterisis loop superimposed with small cycle midlife hysterisis loop

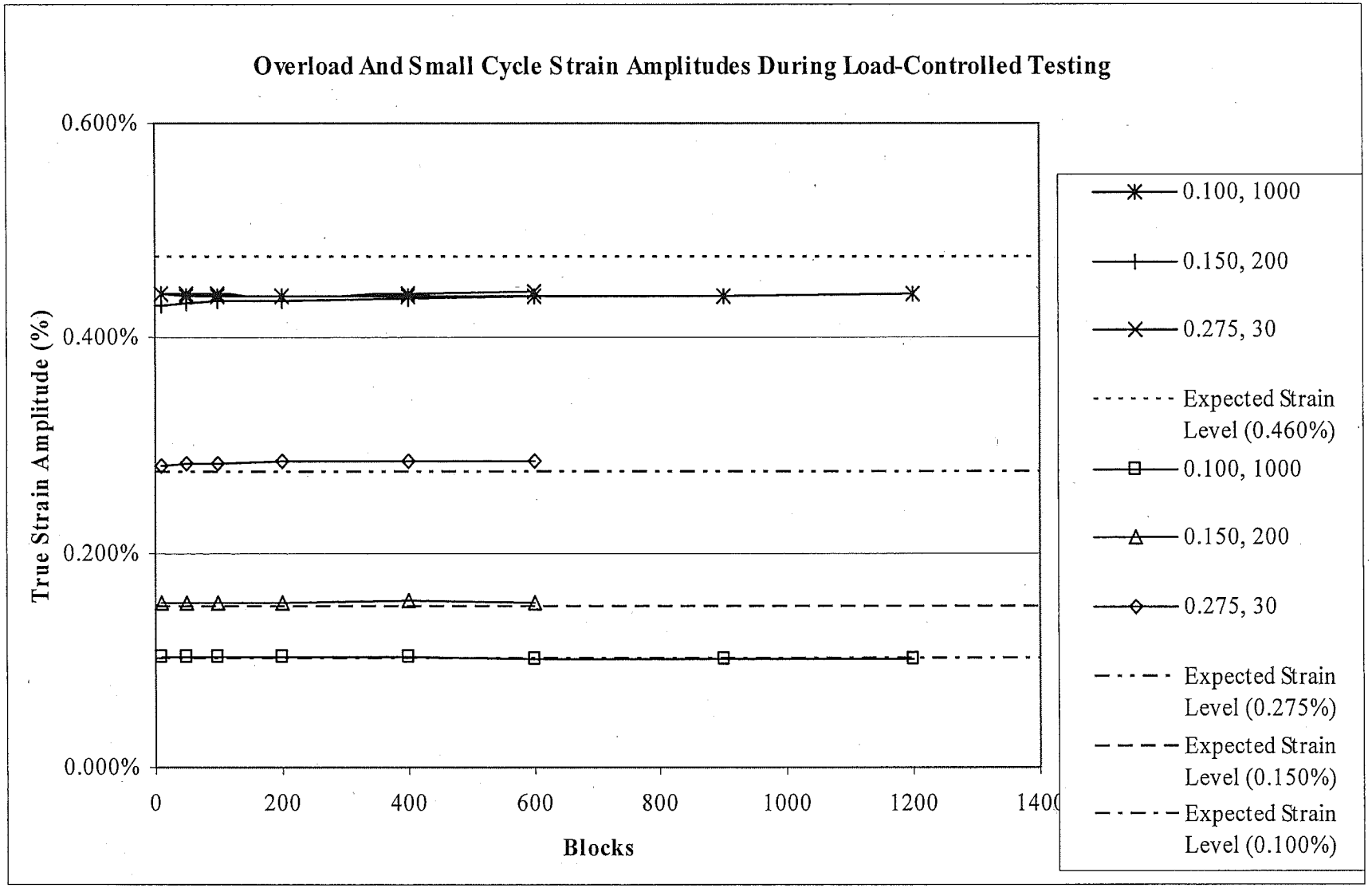

Figure A.7: Comparison between the strain levels recorded during load-controlled periodic overload tests

AppendixB

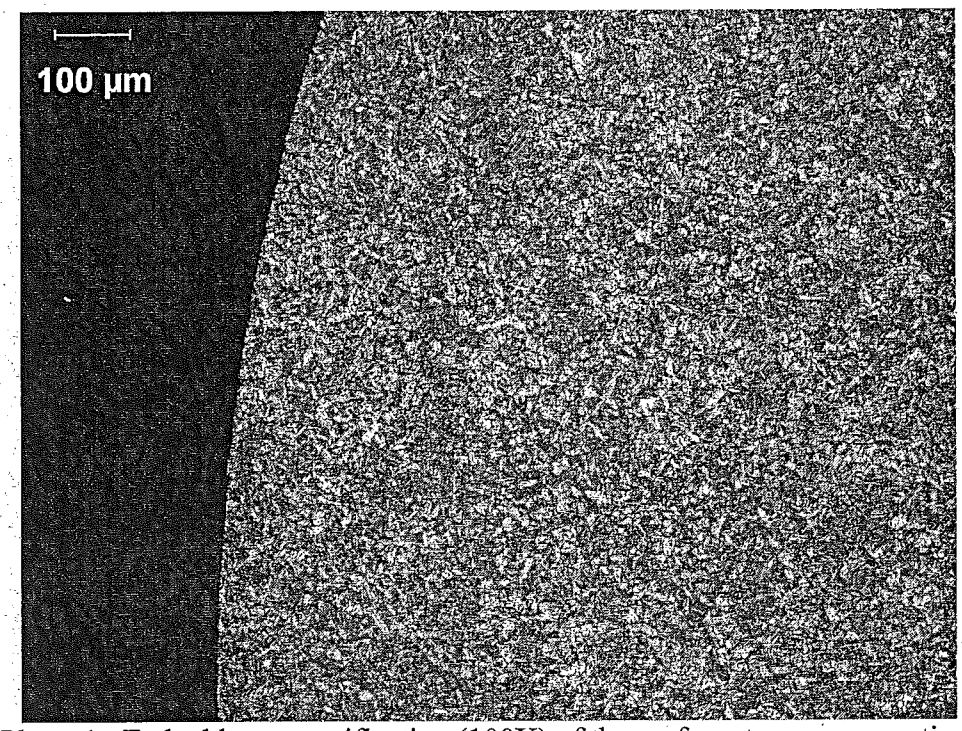

Photo 1: Etched low magnification (100X) of the surface, transverse section.

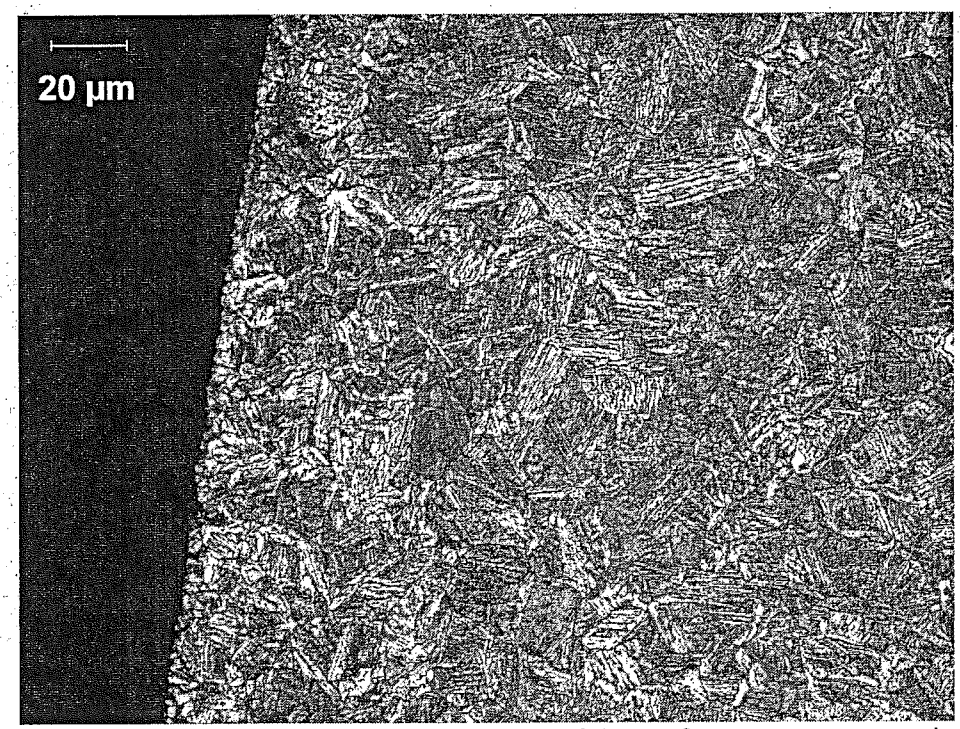

Photo 2: Etched high magnification (500X) of the surface, transverse section.

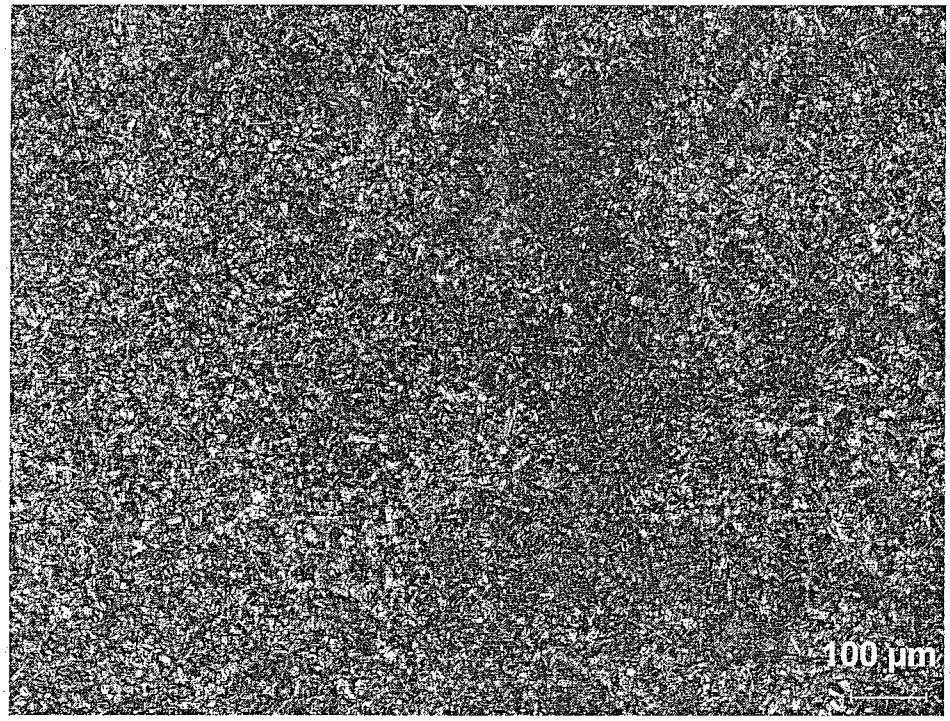

Photo 3: Etched low magnification (100X) of the core, transverse section.

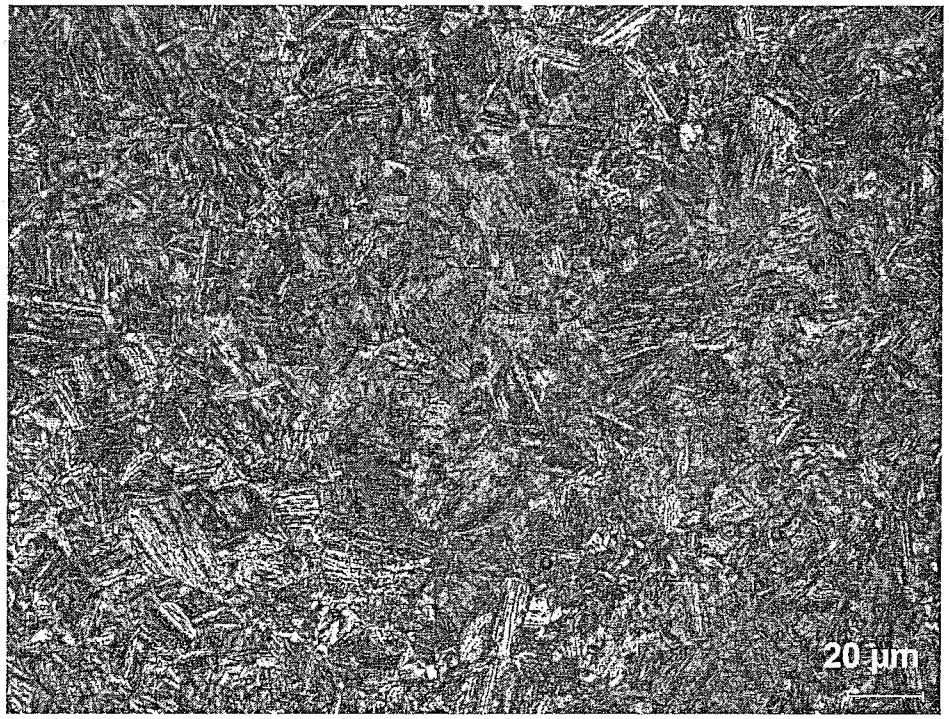

Photo 4: Etched high magnification (500X) of the core, transverse section.

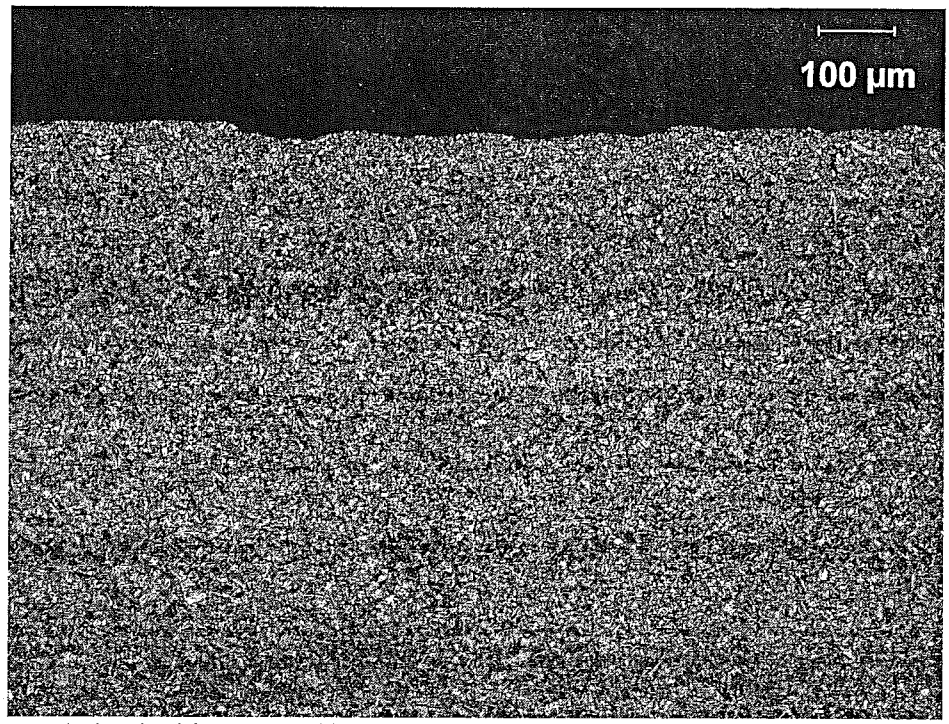

Photo 5: Etched low magnification (100X) of the surface, longitudinal section.

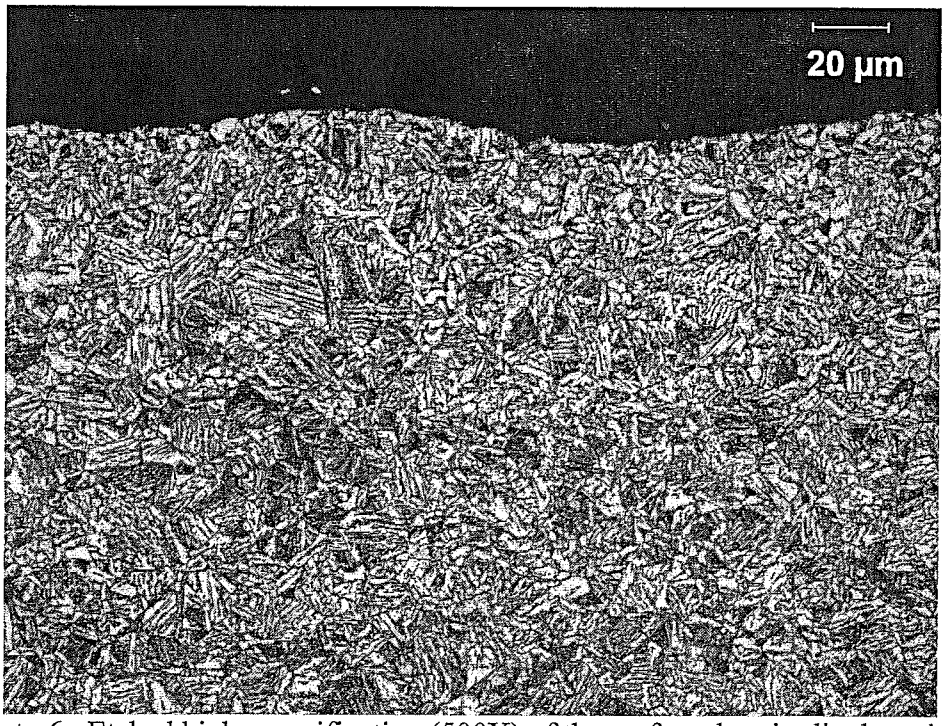

Photo 6: Etched high magnification (500X) of the surface, longitudinal section.

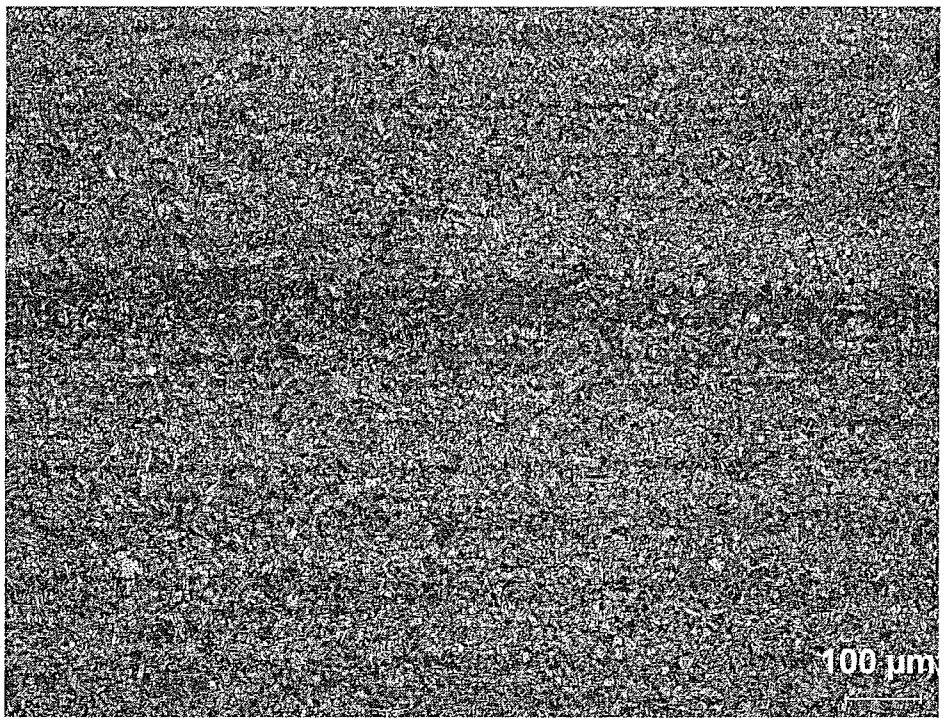

Photo 7: Etched low magnification (100X) of the core, longitudinal section.

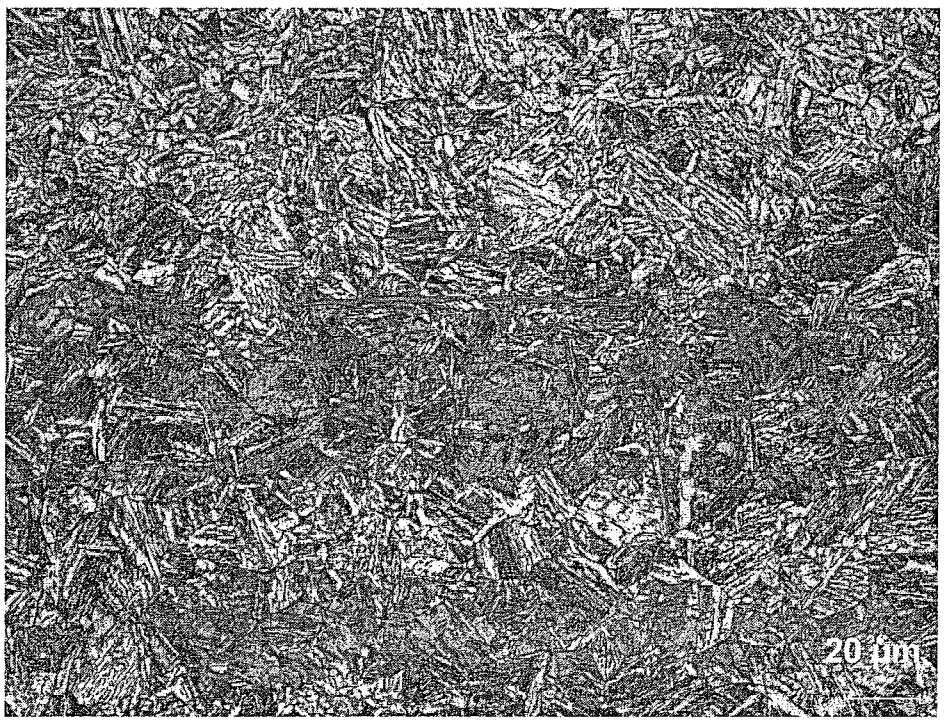

Photo 8: Etched high magnification (500X) of the core, longitudinal section.

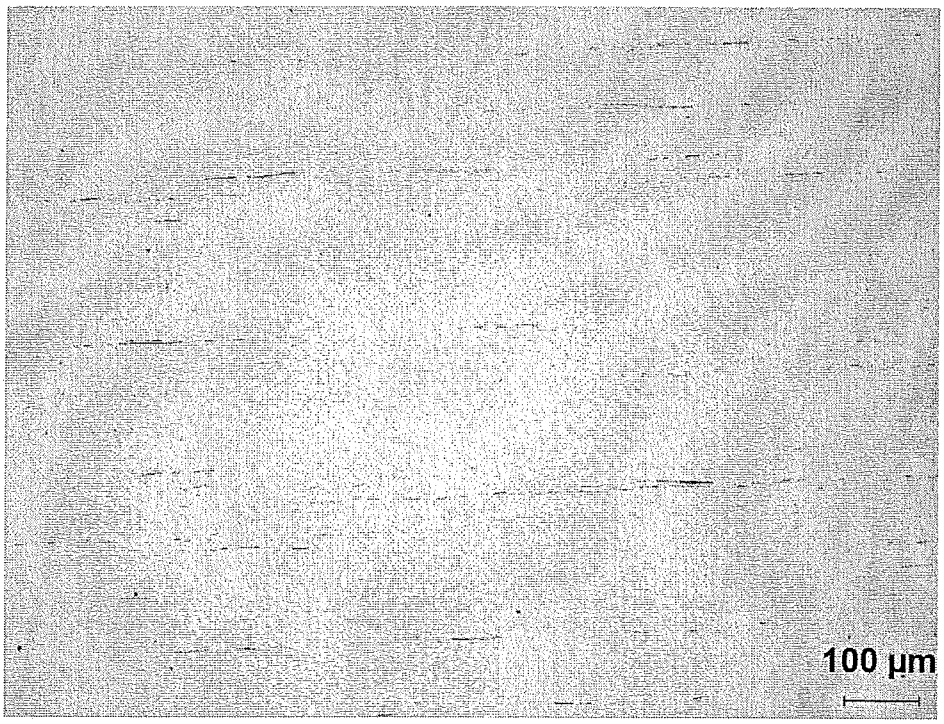

Photo 9: Unetched high magnification (100X) of the core, longitudinal section.